Journal of Medicinal Chemistry



Article

# N-Phenyl-4,5-dibromopyrrolamides and N-Phenylindolamides as ATP competitive DNA Gyrase B Inhibitors: Design, Synthesis, and Evaluation

Nace Zidar, Helena Macut, Tihomir Tomasic, Matjaz Brvar, Sofia Montalvão, Päivi Tammela, Tom J Solmajer, Lucija Peretlin Masic, Janez Ilaš, and Danijel Kikelj

*J. Med. Chem.*, **Just Accepted Manuscript** • DOI: 10.1021/acs.jmedchem.5b00775 • Publication Date (Web): 30 Jun 2015





Journal of Medicinal Chemistry is published by the American Chemical Society. 1155 Sixteenth Street N.W., Washington, DC 20036

# *N*-Phenyl-4,5-dibromopyrrolamides and *N*-Phenylindolamides as ATP Competitive DNA Gyrase B Inhibitors: Design, Synthesis, and Evaluation

*Nace Zidar,[†] Helena Macut,[†] Tihomir Tomašič,[†] Matjaž Brvar,[‡] Sofia Montalvão,[§] Päivi Tammela,[§] Tom Solmajer,[‡] Lucija Peterlin Mašič,[†] Janez Ilaš[†] and Danijel Kikelj*[†]*

[†] Faculty of Pharmacy, University of Ljubljana, Aškerčeva 7, 1000 Ljubljana, Slovenia; [‡] National Institute of Chemistry, Laboratory for Biocomputing and Bioinformatics, 1001 Ljubljana, Slovenia; [§] Centre for Drug Research, Division of Pharmaceutical Biosciences, Faculty of Pharmacy, University of Helsinki, P.O. Box 56 (Viikinkaari 5 E), Helsinki FI-00014, Finland

KEYWORDS: antibacterial; inhibitor; ATP competitive; DNA gyrase B; GyrB; structure-based design; topoisomerase; 4,5-dibromopyrrole.

ABSTRACT

Bacterial DNA gyrase is a well-known and validated target in the design of antibacterial drugs. However, inhibitors of its ATP binding subunit, DNA gyrase B (GyrB), have so far not reached clinical use. In the present study, three different series of *N*-phenyl-4,5-dibromopyrrolamides and *N*-phenylindolamides were designed and prepared as potential

DNA gyrase B inhibitors. The $IC_{50}$ values of compounds on DNA gyrase from *Escherichia coli* were in the low micromolar range, with the best compound, (4-(4,5-dibromo-1*H*-pyrrole-2-carboxamido)benzoyl)glycine (**18a**), displaying an $IC_{50}$ of 450 nM. For this compound a high-resolution crystal structure in complex with *E. coli* DNA gyrase B was obtained, revealing details of its binding mode within the active site. The binding affinities of three compounds with GyrB were additionally evaluated by surface plasmon resonance and the results were in good agreement with the determined enzymatic activities. For the most promising compounds the inhibitory activities against DNA gyrase from *Staphylococcus aureus* and topoisomerases IV from *E. coli* and *S. aureus* were determined. Antibacterial activities of the most potent compounds of each series were evaluated against two Gram-positive and two Gram-negative bacterial strains. The results obtained in this study provide valuable information on the binding mode and structure-activity relationship of *N*-phenyl-4,5-dibromopyrrolamides and *N*-phenylindolamides as promising classes of ATP competitive GyrB inhibitors.

## INTRODUCTION

By the mid-1960s, the major advances of the "antibiotic era" had led to the belief among some scientists that infectious diseases are largely dealt with. These views were reflected in priorities of research funding by the governments and the pharmaceutical industry.[1] The over-optimism of those years was soon followed by the realization that, for every antibacterial drug introduced into the clinic, resistance was quickly developed by bacteria. As a consequence, infectious diseases remain one of the major global health concerns, so new targets and appropriate inhibitory compounds are urgently needed in the fight against resistant microorganisms.[2]

One of the best established and validated targets in antibacterial drug discovery are the bacterial topoisomerases, enzymes essential for control of the topological state of DNA during

cell division and DNA replication.[3] There are two major classes of topoisomerases: type I, that catalyze single strand breaks and type II, that are responsible for the transient break of two strands of DNA.[4] DNA gyrase is a type IIA topoisomerase whose main function is to introduce negative supercoils into the DNA molecule. It is a heterotetrameric protein composed of two A subunits (DNA gyrase A or GyrA) and two B subunits (DNA gyrase B or GyrB). The main role of subunit A is cleavage and reunion of the DNA molecule, while subunit B binds ATP and, through its hydrolysis, provides energy for the cleavage/ligation reactions. A further important bacterial type IIA topoisomerase is topoisomerase IV (topo IV). This plays a critical role in the control of DNA supercoiling and is responsible for unlinking, or decatenating, daughter chromosomal DNA following DNA replication. Topo IV has a heterotetrameric structure similar to that of DNA gyrase, with two ParC subunits homologous to GyrA, and two ParE subunits homologous to GyrB.[5] DNA gyrase and topo IV exhibit 40% overall sequence identity[6] and possess significantly similar active sites.[3b, 7] Currently, the only clinically relevant DNA gyrase/topo IV inhibitors are fluoroquinolones. These bind to the GyrA/ParC subunit, stabilizing the covalent gyrase/topo IV-DNA complexes, thereby preventing the reunion of the two DNA strands, stopping the replication cycle and, ultimately, leading to cell death.[8] Because of some serious side effects and the emergence of fluoroquinolone-resistant bacteria, the clinical use of fluoroquinolones is limited.

An attractive, but so far less successfully exploited target for the design of antibacterials is the ATP binding site of DNA gyrase that is located on the GyrB subunit. It has been shown that the likelihood of cross resistance between fluoroquinolones and ATP competitive inhibitors is low, thus making GyrB an interesting target in the fight against fluoroquinolone resistance. Among the earliest known ATPase inhibitors of DNA gyrase were aminocoumarin natural products such as novobiocin (**1**) and clorobiocin (**2**) (Figure 1a). Novobiocin was introduced into the clinic in the 1960s, but was soon withdrawn because of its acute toxicity

and resistance problems. The binding site of aminocoumarin antibiotics overlaps partially with the ATP binding site and has been characterized from several high resolution crystal structures (Figure 1b).[9] The substituted deoxysugar moiety, novobiose, binds into the adenine part of the ATP binding pocket and interacts with Asp73 (*E. coli* numbering), while the coumarin ring of aminocoumarins is directed away from the ATP binding pocket and makes contact with Arg136.[3c] Though the binding modes of novobiocin and clorobiocin are similar, clorobiocin has a somewhat stronger affinity for GyrB, attributed to the additional interactions formed by the 5-methylpyrrolo-2-carboxylate group of clorobiocin, than those formed by the carbamate group of novobiocin. The methyl group at position 5 of the pyrrole ring forms additional hydrophobic contacts with the residues Val43, Ala47, Val71 and Val 167 in the adenine-binding pocket of the enzyme.[3c]

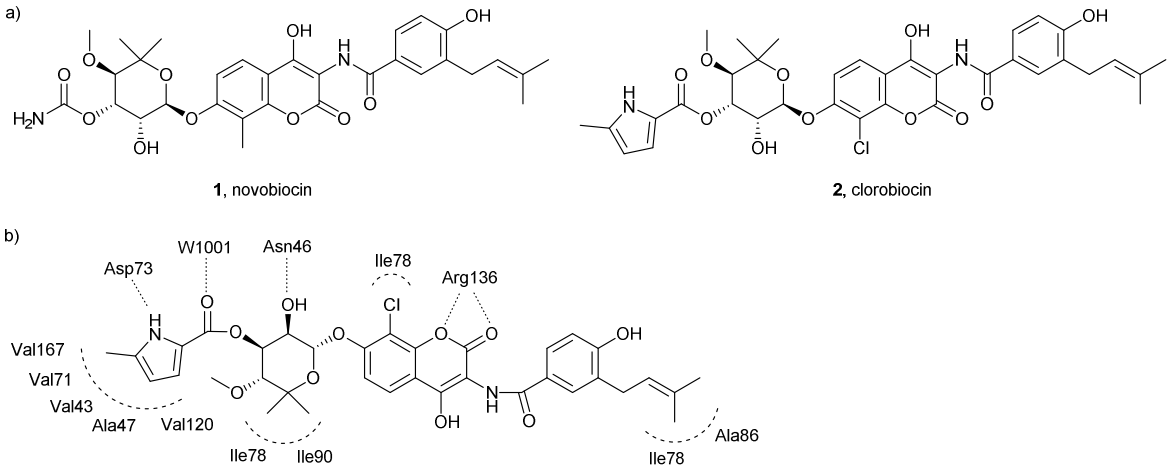


**Figure 1.** (a) Structures of novobiocin (**1**) and clorobiocin (**2**), natural aminocoumarin inhibitors of DNA gyrase B; (b) Schematic representation of interactions between clorobiocin (**2**) and *E. coli* GyrB (PDB code: 1KZN).[9a] H-bonds are indicated by dotted lines. Hydrophobic interactions are shown as dashed curves.

In recent years, there has been extensive research directed at discovering new inhibitors of DNA gyrase B with improved enzyme affinities, more effective antibacterial activities and favorable pharmacokinetic properties. The majority of recently discovered compounds are low-molecular weight ligands, identified through high-throughput screening (HTS) or structure-based virtual screening (VS) campaigns and optimized by structure-based design.[3a, b] Recently discovered GyrB inhibitors belong to a number of chemical classes, such as 4,5'-bithiazoles (**3**),[10] indolin-2-ones (**4**),[11] indazoles (**5**),[12] imidazo[1,2-a]pyridines (**6**),[13] benzimidazole ureas (**7**),[14] pyrazolthiazoles (**8**),[15] azaindoles (**9**),[16] pyrrolopyrimidines (**10**),[17] pyrrolamides (**11**),[18] and tetrahydrobenzothiazoles (**12**)[19] (Figure 2). Their binding modes in the GyrB active sites have been well characterized from several X-ray crystal structures. A common feature of the majority of GyrB inhibitors is a hydrogen bond donor – hydrogen bond acceptor pattern that is essential for the formation of a hydrogen bond network with Asp73 and a conserved water molecule in the adenine-binding pocket. Although several synthetic compounds possess excellent inhibitory activities against DNA gyrase B, none have so far reached the clinic. Further research is needed in order to produce drug candidates with stronger in vitro and in vivo antibacterial activities, less toxicity and good ADME properties. The aim of the present study was to specifically address these problems with the focus on improving the enzymatic activities through a detailed structure-based design.

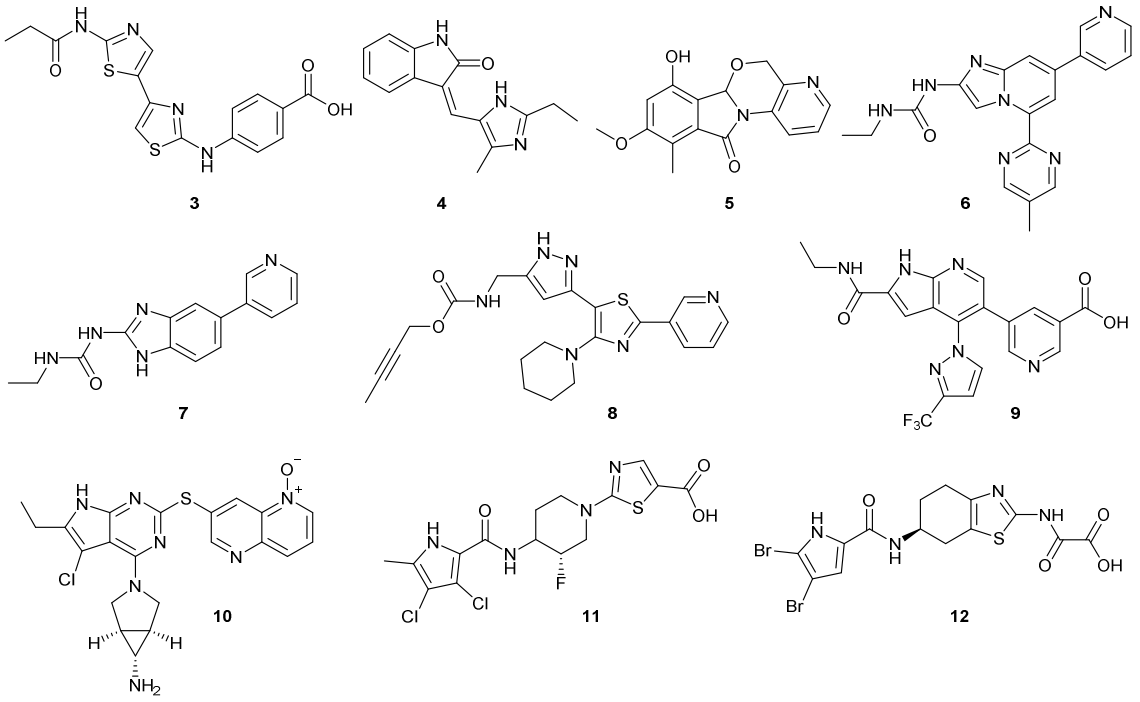


**Figure 2.** Representative synthetic inhibitors of DNA gyrase B from the chemical classes of 4,5'-bithiazoles (**3**),[10] indolin-2-ones (**4**),[11] indazoles (**5**),[12] imidazo[1,2-a]pyridines (**6**),[13] benzimidazole ureas (**7**),[14] pyrazolthiazoles (**8**),[15] azaindoles (**9**),[16] pyrrolopyrimidines (**10**),[17] pyrrolamides (**11**),[18] and tetrahydrobenzothiazoles (**12**)[19]

## RESULTS AND DISCUSSION

**Design.** Three series of *N*-phenyl-4,5-dibromopyrrolamides and *N*-phenylindolamides were designed and prepared as potential DNA gyrase B inhibitors in the course of modification of our 5,6,7,8-tetrahydrobenzothiazole inhibitor series (**12**, Figure 2):[19] (i) compounds with a 4-aminobenzamide central part (**A**, Figure 3), (ii) compounds containing a 4-aminophenol central core (**B**, Figure 3), and (iii) compounds comprising a 4-aminobenzene ring with heterocyclic substituents or basic side chain functionalities (**C**, Figure 3). In all three series of compounds, 4,5-dibromopyrrolamide or indolamide groups were selected to constitute the western part of the inhibitor molecules. The 4,5-dibromopyrrolamide and indolamide moieties

both comprise an essential hydrogen bond donor-acceptor motif, a common feature of the majority of known GyrB inhibitors. The strategy of incorporating substituted pyrrolamides as adenine bioisosteres has been employed successfully in the series of GyrB inhibitors (e.g. **11**) produced at AstraZeneca.[18] 4,5-Dibromopyrrole-2-carboxamide-containing compounds are present in nature, for example in alkaloids oroidin and dibromosceptrin. They are secondary metabolites produced by various marine sponges and exhibit a variety of biological activities.[20] The role of the 4,5-dibromo functionality in binding these compounds is, on the one hand to occupy the hydrophobic pocket of the enzyme and, on the other hand, to increase the acidity of the pyrrole amino group and thus improve its interaction with the Asp73 residue. By replacing the 4,5-dibromopyrrole group with a sterically more bulky indole group, we aimed to explore the size of the hydrophobic pocket in the adenine-binding site. Aniline moiety was introduced as the central core of the molecules. It does not form additional interactions with the enzyme, but is suitable for functionalization with various substituents to produce compounds with the spatial arrangements of functional groups that interact with specific amino acid residues in the active site. On the aniline *para*-position we introduced groups that could make favorable contacts with Arg76 or Arg136. To enable ionic interactions with Arg136 we attached substituents that comprise terminal carboxylic acid functionalities and, in order to explore the optimal lengths of the inhibitors, in type **A** series, analogs with 2, 3 and 4 atoms linkers between the phenyl ring and the COOH group were prepared. To assess the importance of the free carboxylic acid group for biological activity, derivatives with methyl ester functionalities and derivatives in which the carboxylic group was transformed into the primary carboxamide group (Scheme 1, compounds **19a-c**) were prepared and evaluated. To further elucidate the structure-activity relationship (SAR), type **B** derivatives with an additional carboxylic acid substituent on the phenyl ring (Scheme 2, compounds **24b**, **24d**, **25b** and **25d**), and type **C** derivatives with basic side chain functionalities, i.e.,

dimethylamino group (Scheme 3, compound **29a**) and a morpholin-4-yl group (Scheme 3, compound **29b**), were prepared. Finally, to determine whether conformational freedom of the side chain is important for biological activity, compound **35** (Scheme 4) with an (*S*)-4,5-dihydrooxazole-4-carboxylic acid substituent on the *para*-position of the phenyl ring was prepared.

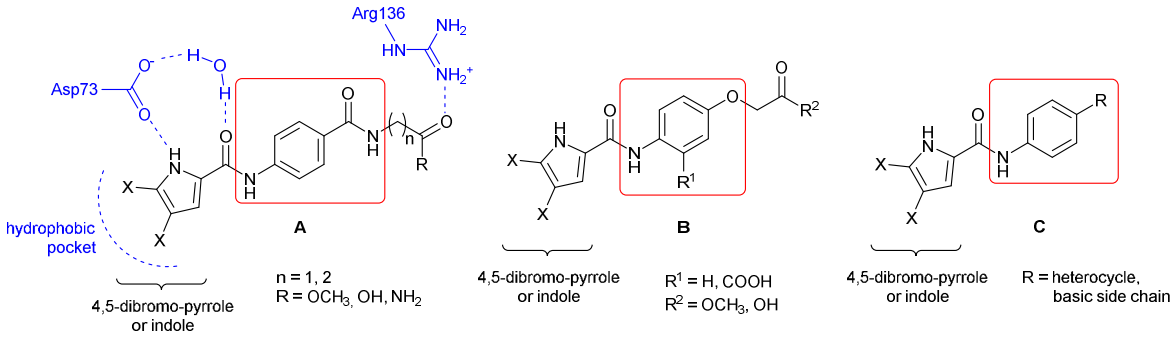


**Figure 3.** Design of *N*-phenyl-4,5-dibromopyrrolamides and *N*-phenylindolamides as ATP competitive DNA gyrase B inhibitors.

**Chemistry.** The synthesis of 4,5-dibromopyrrole- and indole-2-carboxamido-benzamides **18a-d** and **19a-c** is outlined in Scheme 1. In the first step, 4-nitrobenzoyl chloride (**1**) was reacted with glycine or β-alanine methyl ester hydrochloride (**14a** or **14b**) in the presence of potassium carbonate, to afford 4-nitrobenzamides **15a-b**. After reduction of the nitro groups of **15a-b**, the obtained 4-aminobenzamides **16a-b** were coupled with 4,5-dibromo-pyrrole-2-carboxylic acid or indole-2-carboxylic acid in a TBTU-promoted reaction, to give compounds **17a-d**. The target compounds **18a-d** were obtained after hydrolysis of the methyl ester groups with aqueous lithium hydroxide. In derivatives **17a-c** the methyl ester functionalities were further converted to primary carboxamide groups with gaseous $NH_3$, to give **19a-c**.

**Scheme 1. Synthesis of 4-(4,5-dibromo-pyrrole-2-carboxamido)benzamides 18a-b, 19a-b, and 4-(indole-2-carboxamido)benzamides 18c-d, 19c**[a]

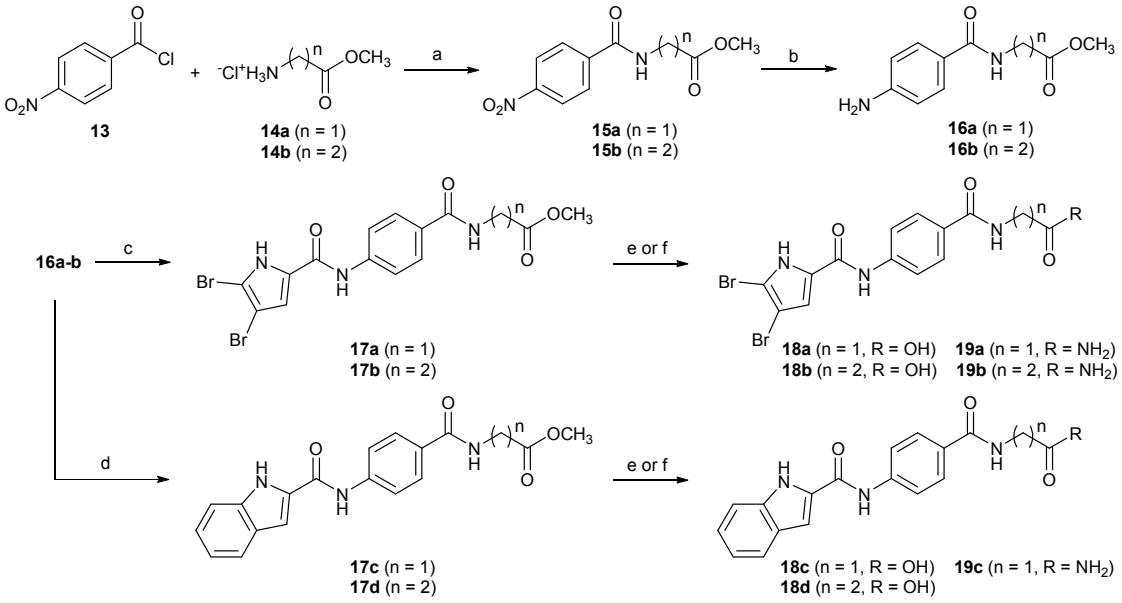


[a]Reagents and conditions: (a) $K_2CO_3$, $CH_3CN$, 0 °C → rt, 15 h; (b) $H_2$, Pd-C, MeOH, rt, 5 h; (c) 4,5-dibromo-pyrrole-2-carboxylic acid, TBTU, NMM, $CH_2Cl_2$, 50 °C, 15 h; (d) indole-2-carboxylic acid, TBTU, NMM, $CH_2Cl_2$, 50 °C, 15 h; (e) LiOH, THF/$H_2O$, 5 h, rt; (f) $NH_{3(g)}$, MeOH/THF, 0 °C → rt, 15 h.

Substituted 2-(4-(4,5-dibromo-pyrrole-2-carboxamido)phenoxy)acetic acids **25a-b** and 2-(4-(indole-2-carboxamido)phenoxy)acetic acids **25c-d** were synthesized according to Scheme 2. After alkylation of the phenolic hydroxyl groups of 4-nitrophenol (**20a**) or methyl 5-hydroxy-2-nitrobenzoate (**20b**) with methyl 2-bromoacetate (**21**) and potassium carbonate as reagents, the products **22a-b** were submitted to catalytic hydrogenation to reduce the aromatic nitro groups to amino groups. TBTU-promoted coupling of **23a-b** with 4,5-dibromo-pyrrole-2-carboxylic acid or indole-2-carboxylic acid, and subsequent hydrolysis of methyl esters gave target compounds **25a-d**.

**Scheme 2. Synthesis of 2-(4-(4,5-dibromo-pyrrole-2-carboxamido)phenoxy)acetic acids 13a-b and 2-(4-(indole-2-carboxamido)phenoxy)acetic acids 25c-d**[a]

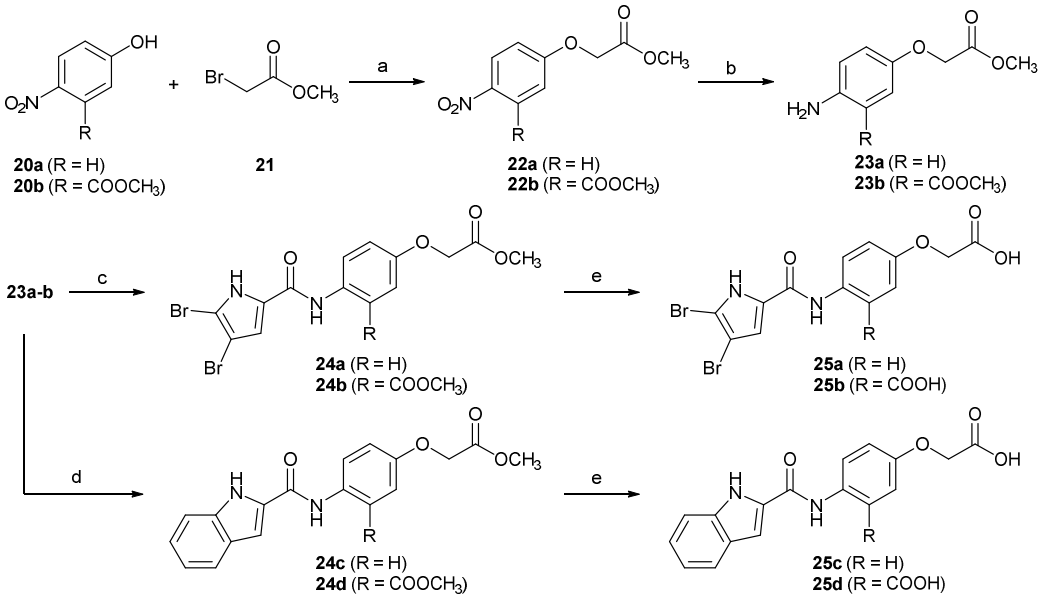


[a]Reagents and conditions: (a) $K_2CO_3$, $CH_3CN$, rt, 15 h; (b) $H_2$, Pd-C, MeOH, rt, 5 h; (c) 4,5-dibromo-pyrrole-2-carboxylic acid, TBTU, NMM, $CH_2Cl_2$, 50 °C, 15 h; (d) indole-2-carboxylic acid, TBTU, NMM, $CH_2Cl_2$, 50 °C, 15 h; (e) LiOH, THF/$H_2O$, 15 h, rt.

The synthetic route to 4,5-dibromo-*N*-(4-ethoxyphenyl)-1*H*-pyrrole-2-carboxamides **29a-b** is presented in Scheme 3. 4-Nitrophenol (**20a**) was reacted with 2-chloro-*N*,*N*-dimethylethylamine hydrochloride (**26a**) or 2-chloroethylmorpholine hydrochloride (**26b**) to afford **27a-b**. After reduction of the nitro groups of **27a-b**, the products **28a-b** were coupled with 4,5-dibromo-pyrrole-2-carboxylic acid to give the target compounds **29a-b**.

**Scheme 3. Synthesis of 4,5-dibromo-*N*-(4-ethoxyphenyl)-1*H*-pyrrole-2-carboxamides 29a-b**[a]

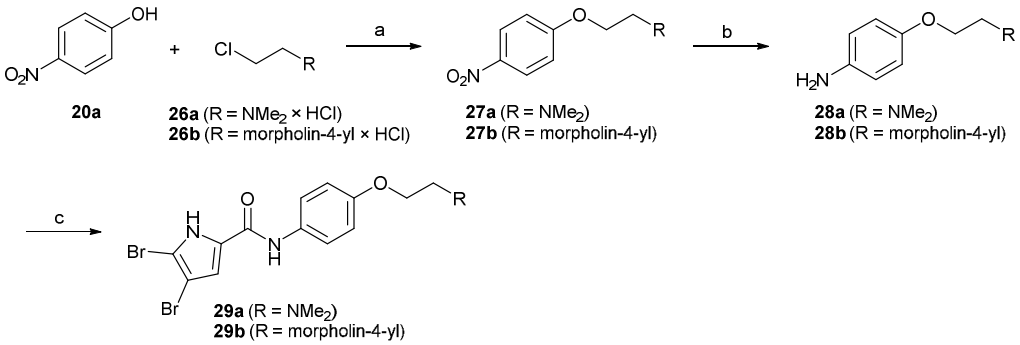


[a]Reagents and conditions: (a) $K_2CO_3$, $CH_3CN$, 50 °C, 15 h; (b) $H_2$, Pd-C, EtOH, rt, 5 h; (c) 4,5-dibromo-pyrrole-2-carboxylic acid, TBTU, NMM, $CH_2Cl_2$, 50 °C, 15 h.

(*S*)-2-(4-(4,5-Dibromo-pyrrole-2-carboxamido)phenyl)-4,5-dihydrooxazole-4-carboxylic acid (**35**) was prepared according to Scheme 4. 4-Nitrobenzonitrile (**30**) was first converted to the imino ester hydrochloride **31** in a Pinner reaction with methanol and hydrochloric acid as reagents. The cyclisation of an imino ester functionality to a 4,5-dihydrooxazole ring (derivative **32**) was performed with L-serine methyl ester hydrochloride in the presence of triethylamine. The nitro group of **32** was then reduced to an amino group and the product **33** coupled with 4,5-dibromo-pyrrole-2-carboxylic acid to give derivative **34**. Hydrolysis of the methyl ester functionality led to the target compound **35**.

**Scheme 4. Synthesis of (*S*)-2-(4-(4,5-dibromo-pyrrole-2-carboxamido)phenyl)-4,5-dihydrooxazole-4-carboxylic acid (35)[a]**

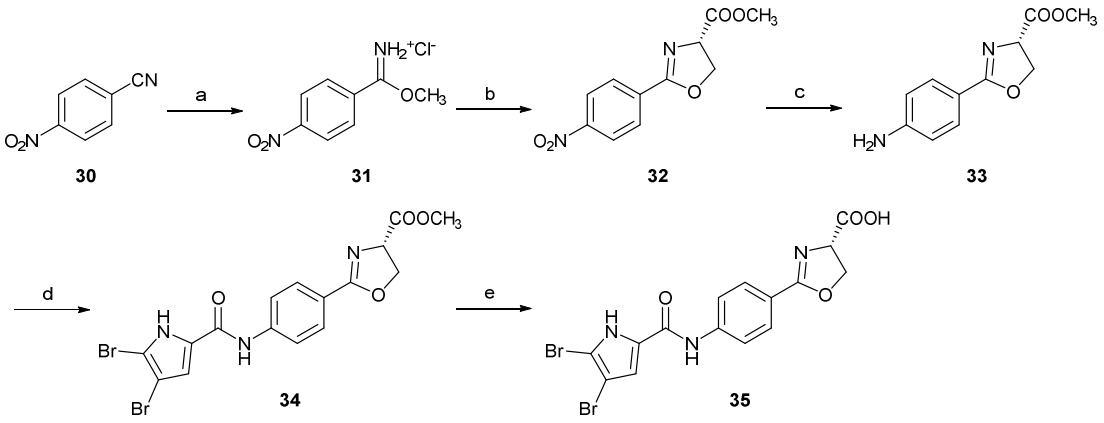


[a]Reagents and conditions: (a) $HCl_{(g)}$, MeOAc/MeOH (10:1), 0 °C → 4 °C, 48 h; (b) L-serine methyl ester hydrochloride, $Et_3N$, $CH_2Cl_2$, rt, 48 h; (c) $H_2$, Pd-C, EtOH, rt, 15 h; (d) 4,5-dibromo-pyrrole-2-carboxylic acid, TBTU, NMM, $CH_2Cl_2$, 50 °C, 15 h; (e) LiOH, MeOH/$H_2O$, 15 h, rt.

**Inhibitory activities against DNA gyrase and topoisomerase IV.** Twenty-one *N*-phenyl-4,5-dibromopyrrolamides and *N*-phenylindolamides of all three structural classes (**A**-**C**, Figure 3) were prepared and evaluated for inhibitory activity against *E. coli* DNA gyrase. The results are presented in Tables 1-3 as $IC_{50}$ values or, for less active inhibitors, as residual activities (RAs) of the enzyme in the presence of 100 μM tested compound. From the results presented in Tables 1 and 2, differences in inhibitory potencies of *N*-phenyl-4,5-dibromopyrrolamide and *N*-phenylindolamide compounds can be observed. The 4,5-dibromopyrrolamide derivatives were always more potent than their indolamide counterparts, indicating that the sterically bulkier indole moiety is unable to occupy optimally the hydrophobic pocket in the adenine binding site, thus making the interactions of the indole NH group with Asp73 less optimal and weaker. Compounds with free carboxylic acid functionalities were generally more potent than their methyl ester precursors, with the only exceptions of compound **18b** (*E. coli* DNA gyrase $IC_{50}$ = 1.4 μM) and its methyl ester derivative **17b** (*E. coli* DNA gyrase $IC_{50}$ = 0.85 μM), where the methyl ester displayed an

approximately 2-fold greater activity. The optimal length of the linker between the phenyl ring and the COOH group could not be established with certainty since, in some cases, the compounds with a three atoms linker were more active than their counterparts with a four atoms linker (comparison of compounds **18a** with 0.45 μM and **18b** with 1.4 μM $IC_{50}$ values). In other cases, longer molecules displayed higher enzymatic activity (comparison of compounds **17a** with 23 μM and **17b** with 0.85 μM $IC_{50}$ values). Compounds in which carboxylic acids were transformed to primary carboxamides (**19a-c**) displayed slightly lower inhibitory activities, as seen from the comparison of compounds **19a** ($IC_{50}$ = 2.2 μM) and **18a** ($IC_{50}$ = 0.45 μM). On the other hand, even though the DNA gyrase activity of **19a** was approximately 5-fold lower than that of compound **18a** the less acidic $CONH_2$ group proved favorable for increasing the compounds' antibacterial activity (Table 2S), probably due to its greater ability to permeate the bacterial cell wall. Compounds **29a** and **29b,** with basic dimethylamino and morpholin-4-yl side chains, did not possess any inhibitory activity. Comparison of compounds **25a** ($IC_{50}$ = 1.4 μM) and **25b** ($IC_{50}$ = 15 μM) shows that introduction of an additional carboxylic substituent to phenyl ring leads to a decrease in inhibitory activity. Apparently, the 2-carboxylic substituent does not form favorable interactions with the enzyme. Compound **35**, with a (*S*)-4,5-dihydrooxazole-4-carboxylic acid substituent on the *para*-position of the phenyl ring and, thus, restrained conformational freedom of the side chain, displayed a promising 5.0 μM $IC_{50}$ value on *E. coli* DNA gyrase.

For the most potent inhibitors of *E. coli* DNA gyrase, also the inhibitory activities against *E. coli* topoisomerase IV, activities against *S. aureus* DNA gyrase and activities against *S. aureus* topoisomerase IV, were determined (Tables 1-3). In general, inhibitory activities against topo IV and DNA gyrase from *S. aureus* were weaker than those against *E. coli* DNA gyrase. The most active inhibitor was compound **18a**, with 58% residual activity on *S. aureus* DNA gyrase and 66% residual activity on *E. coli* topo IV at 100 μM concentrations. The

weaker activity on DNA gyrase from *S. aureus* can be explained by the fact that the adenine-binding pocket of *S. aureus* GyrB is smaller than that of the *E. coli* enzyme. In *E. coli*, Ile51 and Ile175 are replaced by the smaller valines and Leu103 by methionine.[3b] Similarly, the different inhibitory activities of compounds on DNA gyrase and topo IV from the same bacterial species could be explained by a small conformational or dynamic difference in the GyrB and ParE active sites. Although the active sites of GyrB and ParE are very similar, it has been postulated that the replacement of Ile78 in GyrB by Met74 in ParE causes a partial narrowing of the binding pocket and a change in the conformation of the active site, which can result in the altered interaction with inhibitors.[14a, 21]

**Surface Plasmon Resonance (SPR) Experiments.** Compounds **17b**, **18a** and **35**, that showed promising activities in the enzymatic assays, were subjected to surface plasmon resonance (SPR)[22] measurement. $K_d$ values were calculated from the concentration-response curves, using Origin software with a steady state affinity binding model (one site binding). The 24 amino acid long part of the GyrB subunit, G24 protein, which comprises the ATP binding site, was used, with novobiocin as a standard. The measured $K_d$ of 28 nM for novobiocin was in good agreement with 19 nM reported in the literature.[23] All three inhibitors were tested in at least eight concentrations in three parallels, depending on the response of the immobilized protein. The sensorgrams of compounds **17b**, **18a** and **35** at different concentrations are presented in Supporting information Figure 3S. The $K_d$ values for compounds **17b**, **18a** and **35** of 0.97 μM **(**$IC_{50}$ = 0.85 μM**)**, 0.47 μM ($IC_{50}$ = 0.45 μM) and 1.7 μM ($IC_{50}$ = 5.0 μM) are in good agreement with the determined $IC_{50}$ values. These results further validate the *N*-phenyl-4,5-dibromopyrrolamides as an interesting class of DNA gyrase inhibitors and, since only a 24 amino acids long part of the ATP binding GyrB subunit was used for the experiments, they confirm that the tested compounds bind to the enzyme's ATP binding site.

**Table 1.** Inhibitory activities of 4,5-dibromo-*N*-phenyl-1*H*-pyrrole-2-carboxamides and *N*-phenyl-1*H*-indole-2-carboxamides containing a 4-aminobenzamide central part against DNA gyrase and topoisomerase IV.

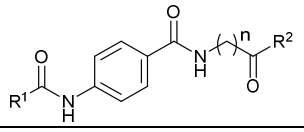

| Compd. | $R^1$ | $R^2$ | n | $IC_{50}$ (μM)[a] or RA (%)[b] | | | |
|---|---|---|---|---|---|---|---|
| | | | | *E. coli* gyrase | *S. aureus* gyrase | *E. coli* topo IV | *S. aureus* topo IV |
| **17a** | 4,5-Dibromo-pyrrol-2-yl | $OCH_3$ | 1 | 23 ± 6 μM | n.d. | n.d. | n.d. |
| **17b** | 4,5-Dibromo-pyrrol-2-yl | $OCH_3$ | 2 | 0.85 ± 0.10 μM<br>$K_d$ = 0.97 ± 0.12 μM[c] | 138% | 100% | 107% |
| **17c** | Indol-2-yl | $OCH_3$ | 1 | 90% | n.d. | n.d. | n.d. |
| **17d** | Indol-2-yl | $OCH_3$ | 2 | 91% | n.d. | n.d. | n.d. |
| **18a** | 4,5-Dibromo-pyrrol-2-yl | OH | 1 | 0.45 ± 0.08 μM<br>$K_d$ = 0.47 ± 0.15 μM[c] | 58% | 66% | 100% |
| **18b** | 4,5-Dibromo-pyrrol-2-yl | OH | 2 | 1.4 ± 0.4 μM | 78% | 61% | 99% |
| **18c** | Indol-2-yl | OH | 1 | 20 ± 6 μM | n.d. | n.d. | n.d. |
| **18d** | Indol-2-yl | OH | 2 | 23 ± 5 μM | n.d. | n.d. | n.d. |
| **19a** | 4,5-Dibromo-pyrrol-2-yl | $NH_2$ | 1 | 2.2 ± 0.3 μM | 90% | 102% | 99% |
| **19b** | 4,5-Dibromo-pyrrol-2-yl | $NH_2$ | 2 | 43% | n.d. | n.d. | n.d. |
| **19c** | Indol-2-yl | $NH_2$ | 1 | 109% | n.d. | n.d. | n.d. |
| **1**[d] | / | / | / | 0.17 ± 0.02 μM | 0.041 ± 0.07 μM | 11 ± 2 μM | 27 ± 7 μM |

[a] Concentration of compound (mean ± SD) that inhibits the enzyme activity by 50%.
[b] Residual activity of the enzyme at 100 μM of the compound.
[c] Dissociation constant (mean ± SD) determined from surface plasmon resonance experiments.
[d] Novobiocin.
n.d. = not determined

**Table 2.** Inhibitory activities of 4,5-dibromo-*N*-phenyl-1*H*-pyrrole-2-carboxamides and *N*-phenyl-1*H*-indole-2-carboxamides containing a 4-aminophenol central part against DNA gyrase and topoisomerase IV.

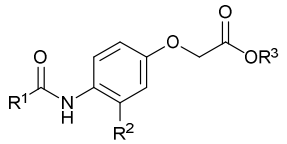

| Compd | $R^1$ | $R^2$ | $R^3$ | $IC_{50}$ (μM)[a] or RA (%)[b] | | | |
|---|---|---|---|---|---|---|---|
| | | | | *E. coli* gyrase | *S. aureus* gyrase | *E. coli* topo IV | *S. aureus* topo IV |
| **24a** | 4,5-Dibromo-pyrrol-2-yl | H | $CH_3$ | 88 ± 19 μM | n.d. | n.d. | n.d. |
| **24c** | Indol-2-yl | H | $CH_3$ | 71% | n.d. | n.d. | n.d. |
| **25a** | 4,5-Dibromo-pyrrol-2-yl | H | H | 1.4 ± 0.2 μM | 100% | 88% | 100% |
| **25b** | 4,5-Dibromo-pyrrol-2-yl | COOH | H | 15 ± 3 μM | n.d. | n.d. | n.d. |
| **25c** | Indol-2-yl | H | H | 47 ± 5 μM | n.d. | n.d. | n.d. |
| **25d** | Indol-2-yl | COOH | H | 78% | n.d. | n.d. | n.d. |
| **1**[c] | / | / | / | 0.17 ± 0.02 μM | 0.041 ± 0.07 μM | 11 ± 2 μM | 27 ± 7 μM |

[a] Concentration of compound (mean ± SD) that inhibits the enzyme activity by 50%.
[b] Residual activity of the enzyme at 100 μM of the compound.
[c] Novobiocin.
n.d. = not determined

**Table 3.** Inhibitory activities of 4,5-dibromo-*N*-phenyl-1*H*-pyrrole-2-carboxamides and *N*-phenyl-1*H*-indole-2-carboxamides containing a central aniline moiety with heterocyclic substituents or basic side chain functionalities against DNA gyrase and topoisomerase IV.

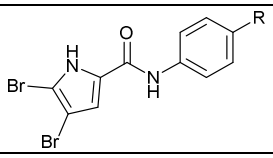


| Compd | R | $IC_{50}$ (μM)[a] or RA (%)[b] | | | |
|---|---|---|---|---|---|
| | | *E. coli* gyrase | *S. aureus* gyrase | *E. coli* topo IV | *S. aureus* topo IV |
| **29a** | 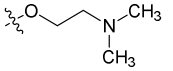 | 94% | n.d. | n.d. | n.d. |
| **29b** | 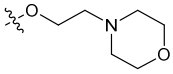 | 88% | n.d. | n.d. | n.d. |
| **34** | 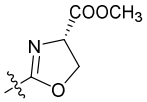 | 50% | n.d. | n.d. | n.d. |
| **35** | 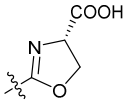 | 5.0 ± 1.1 μM<br>$K_d$ = 1.7 ± 0.3 μM[c] | 83% | 105% | 98% |
| **1**[d] | / | 0.17 ± 0.02 μM | 0.041 ± 0.07 μM | 11 ± 2 μM | 27 ± 7 μM |

[a] Concentration of compound (mean ± SD) that inhibits the enzyme activity by 50%.
[b] Residual activity of the enzyme at 100 μM of the compound.
[c] Dissociation constant (mean ± SD) determined from surface plasmon resonance experiments.
[d] Novobiocin.
n.d. = not determined

**Antibacterial Activity.** The antibacterial activities of the most potent compounds of each series were evaluated against two Gram-positive (*S. aureus* ATCC 25923, *E. faecalis* ATCC 29212) and two Gram-negative (*E. coli* ATCC 25922, *P. aeruginosa* ATCC 27853) bacterial strains (Supporting information, Table 2S). Except for compound **19a**, that showed 23% inhibition of growth of Gram-negative *P. aeruginosa* at 50 μM concentration after 24 h incubation, none of the tested compounds displayed significant antibacterial activity. The higher antibacterial activity of compound **19a** can be attributed to the more favorable physico-chemical properties for bacterial cell entry that are due to the presence of the less acidic primary carboxamido functionality than that of the carboxylic acid group. These results are in accordance with the recently reported linear correlation between activity (pMIC) of compounds on *S. pneumoniae* and their $pK_a$.[24]

**X-Ray Crystallography.** The structure of the 43 kDa N-terminal fragment of *E. coli* DNA gyrase B (GyrB43) in complex with ligand **18a** solved at a resolution of 2.20 Å (PDB code: 4ZVI) revealed the detailed binding mode of the ligand (Figure 4). The structure of *E. coli* GyrB adopts a bilobal architecture, with the ligand bound to the ATP binding site of the N-terminal lobe. The crystals contain one monomer of GyrB in the asymmetric unit and the model comprises residues Leu16 to Thr392, except for the ones indicated in Supporting information Table 1S. The amino acid residues forming the ligand binding site and the ligand are well defined in the electron density map and show clearly the binding mode and the orientation and conformation of the ligand bound to its binding site. Based on a distance of less than 3.5 Å between the donor and acceptor atoms, two specific hydrogen bonds of the ligand **18a** to the side chain atoms of Arg76 and Asp73 were identified. By the same criteria, the presence of additional hydrophilic interactions between the main chain atoms of Thr165 and ligand **18a**, as well as the interactions between side chain atoms of Asp73, Thr165, and Asn46 and ligand **18a** bridged by water molecules, are suggested. The water molecules and

all atoms involved in the formation of hydrogen bonds are well defined by the electron density. The following residues are present in the vicinity of the ligand at distances of 3.9 Å or less: Asn46, Glu50, Asp73, Arg76, Gly77, Ile78, Pro79, Val120, Thr165, and Val167. The weak electron density in this area indicates that the conformation of the carboxylate group of the ligand is flexible.

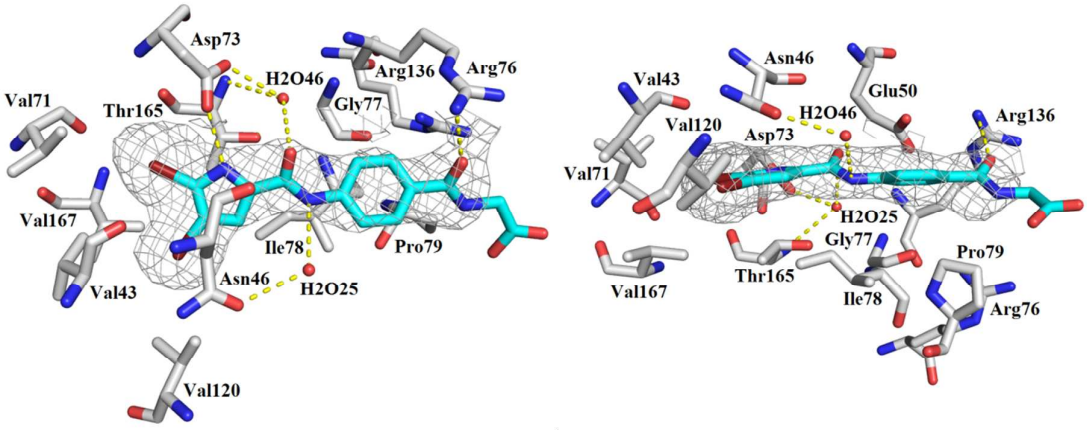


**Figure 4.** X-ray crystal structure of *E. coli* DNA gyrase B in complex with ligand **18a** (PDB code: 4ZVI) shown in two orientations rotated by 90 degrees. The ligand and neighboring protein side chains are shown as stick models, colored according to the chemical atom type ($C_{\mathbf{18a}}$ in cyan, $C_{GyrB}$ in grey, N in blue, O in red, and Br in brown). The conserved water molecule is presented as a red ball. The ligand molecule is shown superimposed with the refined 2Fo-Fc electron density map contoured at 1.0 σ. Hydrogen bonds are indicated as green dotted lines. The Figure was prepared by PyMOL.[25]

**Molecular modeling.** In the structure of *E. coli* DNA gyrase B in complex with inhibitor **18a** the terminal carboxylate group of **18a** is flexible and is not in contact with Arg136 side chain, as designed and predicted by molecular docking (Figure 5a) using FRED software.[26,27] Since only weak electron density is present for the carboxylate group of **18a** and because its conformation is contrary to our expectations, we conducted a molecular dynamics simulation to study the flexibility of the inhibitor in the binding site and to assess whether the carboxylate group of **18a** is able to interact with the Arg136 side chain during the simulation.

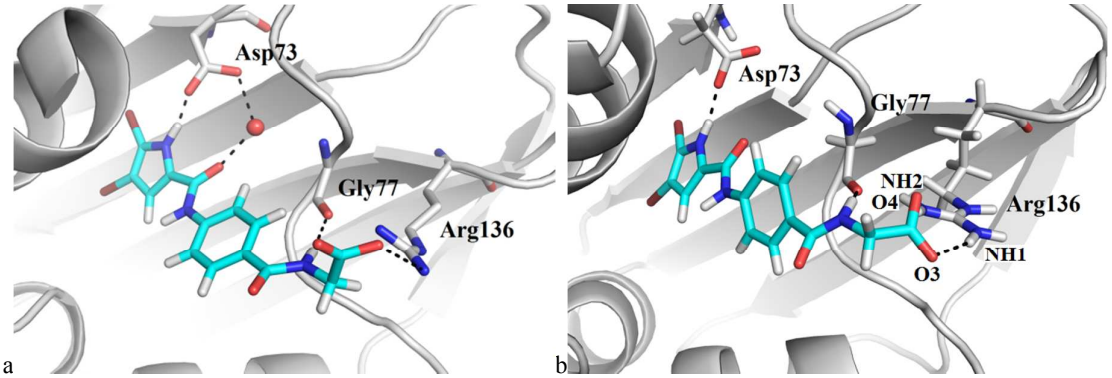


**Figure 5**. a) The binding mode of inhibitor **18a** (in cyan sticks) in the ATP binding site of *E. coli* DNA gyrase B (PDB code: 4DUH, in grey) predicted by docking, and b) the conformation of the GyrB43-**18a** complex at the end of MD simulation (PDB code: 4ZVI). For clarity, only side chains forming hydrogen bonds with inhibitor are presented. The conserved water molecule is presented as red ball. Hydrogen bonds are indicated as black dotted lines. The Figure was prepared by PyMOL.[25]

First, in order to conduct the molecular dynamics study, the completeness of the X-ray structure was improved by homology modeling of the missing loop (residues 99-117) and residues with incomplete side chains, using *E. coli* topoisomerase IV ParE subunit structure (PDB entry: 4HZ0)[17a] as a template and MODELLER 9.13[28] as homology modeling software. Amino acid sequences were aligned using T-COFFEE server[29] and the sequence alignment used as obtained. Ten homology models were generated; the one used for further studies was selected based on DOPE score and stereochemical quality as evaluated by Procheck[30] and ProSA-web[31] server.

The GyrB43-**18a** complex was first solvated using the TIP3P water model and then subjected to a 12 ns molecular dynamics simulation consisting of a 1 ns equilibration run with protein and inhibitor constrained, followed by a 1 ns equilibration run with protein and inhibitor released; the final 10 ns production was then run. The volume, temperature and total energy parameters of the system showed that these parameters were stable during the

production run, confirming the physical stability of the MD simulation (Figure 1S). The RMSD of the protein backbone atoms, that provides information about the structural stability of the system during the MD simulation, increased gradually during equilibration of the system and then remained fairly stable at between 1.5 Å and 2.5 Å (Figure 6a). In contrast, inhibitor **18a** was more flexible than the protein backbone, with greater fluctuation of the RMSD values, between 0.5 Å and 3.2 Å (Figure 6a). Visual inspection of MD trajectory shows that the pyrrolamide moiety of the inhibitor is, as expected, the least flexible part of the molecule, since it is buried deep in the hydrophobic pocket of the ATP binding site. Analysis of the hydrogen bond formation between the pyrrole NH and carboxylate groups of Asp73 shows that the distance between these two groups remains approximately 2 Å throughout the simulation, indicating the stability of this hydrogen bond (Figure 6b). In contrast, the hydrogen bond formation between Arg136 side chain and the carboxylate group of **18a** shows a distribution of distances between 2.8 Å and 15.5 Å (Figure 6b), when monitored by measuring the distances between Arg136NH1 and carboxylate O3 of **18a**, Arg136NH1 and carboxylate O4 of **18a**, Arg136NH2 and carboxylate O3 of **18a**, and Arg136NH2 and carboxylate O4 of **18a** (Figure 2S). This confirms the flexibility of the carboxylate group of **18a** suggested by X-ray diffraction, and shows that it is in contact with the surrounding solvent most of the simulation time. However, if 3.5 Å is taken as the distance threshold for hydrogen bond formation, the carboxylate group of **18a** is in contact with Arg136 side chain for 34% of the simulation time (i.e. between 6.5 ns and 9 ns) (Figure 6b). The conformation of the GyrB43-**18a** complex at the end of MD simulation, in which the carboxylate group of **18a** and the guanidine group of Arg136 interact, is shown in Figure 5b. It closely resembles that obtained by docking (Figure 5a), since hydrogen bonds are formed with Asp73, Gly77 and Arg136.

Thus, MD simulation of the GyrB43-**18a** complex confirms the flexibility of the terminal carboxylate group of **18a**, but also suggests the possibility of its interaction with Arg136, which is not evident from the X-ray structure of the complex. Since the carboxylate group of **18a** is, for most of the simulation time, in contact only with the solvent and not with Arg136 side chain, a less flexible moiety with a better directed hydrogen bond could improve the binding affinity of this type of inhibitors.

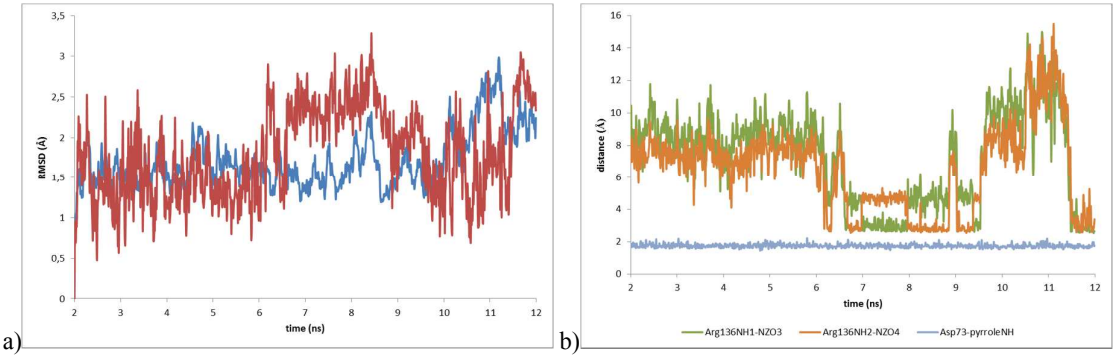


**Figure 6.** a) Backbone RMSD (in blue) and ligand **18a** RMSD (in red) *vs* time plots during the MD simulation of *E. coli* DNA gyrase B in complex with **18a**. b) Distance *vs* time plots between selected GyrB residues and inhibitor **18a** carboxylate and pyrrole NH groups. For clarity, only 3 distance measurements are presented.

## CONCLUSION

Twenty-one new *N*-phenyl-4,5-dibromopyrrolamides and *N*-phenylindolamides were designed and prepared as ATP competitive DNA gyrase B inhibitors and their inhibitory activities on DNA gyrase from *E. coli* were measured. Five compounds displayed $IC_{50}$ values lower than 3 μM and the most active compound, **18a**, had an $IC_{50}$ of 450 nM. The $K_d$ values obtained from SPR for the binding of compounds **17b**, **18a** and **35** to the G24 protein that contains an ATPase domain, were in good agreement with the determined $IC_{50}$ values, which confirmed that the tested compounds bind to the enzyme's ATP binding site. The X-ray crystal structure of compound **18a** in complex with GyrB was resolved, revealing details of its

binding mode within the active site and confirming the rational of our design strategy. Even though the crystal structure showed that the terminal carboxylate of **18a** is flexible and is not in contact with Arg136 side chain, the MD simulation of GyrB43-**18a** complex indicates the possibility of this interaction. From the MD data it can be concluded that a less flexible moiety with a better directed hydrogen bond could improve the binding affinity of inhibitors. The inhibitory activities against DNA gyrase from *S. aureus*, topoisomerase IV from *E. coli* and topoisomerase IV from *S. aureus* were generally weaker than those against *E. coli* DNA gyrase, probably due to differences of the enzymes' active sites. To obtain compounds with stronger in vitro and in vivo antibacterial effectiveness, optimization of their physico-chemical properties, e.g. by increasing the pKa value of the functionalities that interact with Arg76 or Arg136, is suggested. Overall, the structure-activity relationships derived from *E. coli* DNA gyrase inhibitory activities and the information gained from the co-crystal structure of compound **18a** in the active site of GyrB provide a good foundation for the further search for new improved DNA gyrase inhibitors.

## EXPERIMENTAL SECTION

**Determination of Inhibitory Activities on *E. coli* and *S. aureus* DNA Gyrase.** The assay for the determination of $IC_{50}$ values (Inspiralis) was performed on the black streptavidin-coated 96-well microtiter plates (Thermo Scientific Pierce). The plates were first rehydrated with the supplied wash buffer [20 mM Tris-HCl (pH 7.6), 137 mM NaCl, 0.01% (w/v) BSA, 0.05% (v/v) Tween 20] and biotinylated oligonucelotide was immobilized onto the wells. The excess of oligonucleotide was then washed off, and the enzyme assay was carried out in the wells. The final reaction volume of 30 µL in buffer [35 mM Tris × HCl (pH 7.5), 24 mM KCl, 4 mM $MgCl_2$, 2 mM DTT, 1.8 mM spermidine, 1 mM ATP, 6.5 % (w/v) glycerol, 0.1 mg/mL albumin] contained 1.5 U of gyrase from *E. coli* or *S. aureus*, 0.75 µg of relaxed pNO1

plasmid, and 3 μL of inhibitors solution in 10% DMSO and 0.008% Tween 20. Reactions were incubated for 30 min at 37 °C and after the addition of the TF buffer [50 mM NaOAc (pH 5.0), 50 mM NaCl and 50 mM $MgCl_2$] which terminated the enzymatic reaction for another 30 min at rt to allow the triplex formation (biotin-oligonucleotide-plasmid). Afterwards, the unbound plasmid was washed off using TF buffer and the solution of SybrGOLD stain in T10 buffer [10 mM Tris × HCl (pH 8.0) and 1 mM EDTA] was added. After mixing the fluorescence (excitation: 485 nm, emission: 535 nm) was read using a BioTek's Synergy H4 microplate reader. Preliminary screening was performed at inhibitor concentrations of 100 and 10 μM. For most potent compounds $IC_{50}$ was determined with 7 concentrations of the inhibitors. $IC_{50}$ values were calculated using GraphPad Prism software and represent the concentration of inhibitor where the residual activity of the enzyme is 50%. All compounds were assayed in three independent measurements and a final result is given as their average value. Novobiocin [$IC_{50}$ = 0,17 μM (lit. 0,08 μM)[32] for *E. coli* gyrase and $IC_{50}$ = 0,041 μM (lit. 0,01 μM)[32] for *S. aureus* gyrase] was used as the internal standard.

**Determination of Inhibitory Activities on *E. coli* and *S. aureus* Topoisomerase IV.** The assay for the determination of $IC_{50}$ values (Inspiralis) was performed on the black streptavidin-coated 96-well microtiter plates (Thermo Scientific Pierce). The plates were first rehydrated with the supplied wash buffer [20 mM Tris-HCl (pH 7.6), 137 mM NaCl, 0.01% (w/v) BSA, 0.05% (v/v) Tween 20] and biotinylated oligonucelotide was immobilized onto the wells. The excess of oligonucleotide was then washed off, and the enzyme assay was carried out in the wells. The final reaction volume of 30 μL in buffer [40 mM HEPES KOH (pH 7.6), 100 mM potassium glutamate, 10 mM magnesium acetate, 10 mM DTT, 1 mM ATP, 0.05 mg/mL albumin] contained 1.5 U of topoisomerase IV from *E. coli* or *S. aureus*, 0.75 μg of supercoiled pNO1 plasmid, and 3 μL of inhibitors solution in 10% DMSO and 0.008% Tween 20. Reactions were incubated for 30 min at 37 °C and after the addition of the

TF buffer [50 mM NaOAc (pH 5.0), 50 mM NaCl and 50 mM $MgCl_2$] which terminated the enzymatic reaction for another 30 min at rt to allow the triplex formation (biotin-oligonucleotide-plasmid). Afterwards, the unbound plasmid was washed off using TF buffer and the solution of SybrGOLD stain in T10 buffer [10 mM Tris-HCl (pH 8.0) and 1 mM EDTA] was added. After mixing the fluorescence (excitation: 485 nm, emission: 535 nm) was read using a BioTek's Synergy H4 microplate reader. Preliminary screening was performed at inhibitor concentrations of 100 and 10 μM. For most potent compounds $IC_{50}$ was determined with 7 concentrations of the inhibitors. $IC_{50}$ values were calculated using GraphPad Prism software and represent the concentration of inhibitor where the residual activity of the enzyme is 50%. The assays for all compounds were run in triplicate and a final result is given as their average value. Novobiocin [$IC_{50}$ = 11 μM (lit. 10 μM)[32] for *E. coli* topoisomerase IV and $IC_{50}$ = 27 μM (lit. 20 μM)[32] for *S. aureus* topoisomerase IV] was used as the internal standard.

**Surface Plasmon Resonance (SPR) Measurements.** Surface plasmon resonance (SPR) measurements were performed on a Biacore T100 machine using CM5 sensor chip (Biacore, GE Healthcare). The system was primed twice with running buffer (10 mM Hepes, 150 mM NaCl, 3 mM EDTA, 0.005% surfactant P20, pH 7.4). The G24 protein was immobilized on the second flow cell of a sensor chip CM5 using standard amino coupling method. The carboxymethylated dextran layer was activated with 7 min pulse of 1-ethyl-3-(3-dimethylaminopropyl)-carbodiimide (EDC) and *N*-hydroxysuccinimide (NHS) mixed in a 1:1 ratio. Protein was diluted to the final concentration of 50 μg/mL in 10 mM sodium acetate (pH 4.5) and injected in two short pulses to reach the final immobilization level around 18.000 response units. Finally, the rest of the surface was deactivated with 7 min injection of ethanolamine. The first flow cell was activated with EDC/NHS and deactivated with ethanolamine and served as a reference cell for subtraction of nonspecific binding. The activity of the chip was tested and confirmed using novobiocin as a standard. Measured $K_d$ for

novobiocin was 28 nM (lit. 19 nM).[23] Analytes were prepared as DMSO 100× stock solutions and were diluted with a running buffer prior to the injection. They were injected at a flow rate of 30 μL/min for 90 s, and dissociation was monitored for additional 120 s. Since the dissociation of analytes from the ligand was rapid, no regeneration protocol was needed. For the titration of analytes, the 1% of the DMSO was added to the running buffer in order to diminish the difference in a refractive index between the samples and running buffer. All three inhibitors (**17b**, **18a** and **35**) were tested in at least eight different concentrations in three parallel titrations. The sensorgrams (Supporting Information, Figure 3S) were analyzed using BiaEval software (Biacore, GE Healthcare). The equilibrium binding responses were determined from the binding levels 5 s before the stop of the injection. $K_d$ values were determined by the fitting of the data to 1:1 steady state binding model as described in Results.

**Determination of Antibacterial Activity.** Clinical control strains of *Enterococcus faecalis* (Gram-positive, ATCC 29212), *Staphylococcus aureus* (Gram-positive, ATCC 25923), *Escherichia coli* (Gram-negative, ATCC 25922) and *Pseudomonas aeruginosa* (Gram-negative, ATCC 27853), were obtained from Microbiologics Inc. (St. Cloud, Minnesota, USA). Bacterial cultures were initiated on MH agar (Becton Dickinson, Franklin Lakes, NJ, USA) slants and prior to the assays, suspensions were prepared into MH II broth (Becton Dickinson, Franklin Lakes, NJ, USA) and incubated at 37 °C for 16–20 h at 100 rpm. Antimicrobial assays were performed by the broth microdilution method in 96-well plate format according to the CLSI guidelines.[33] Briefly, bacterial suspension was diluted with MHB to obtain a final inoculum of $5 \times 10^5$ CFU/mL in the assay. An equal volume of bacterial suspension and test compound solution diluted into assay media were mixed together in the plate and incubated for 24 h at 37 °C. Absorbance values measured at 620 nm were used for evaluating the antimicrobial effects of test compounds by comparing to untreated controls and expressed as percentage inhibition of growth. Reference antibiotics were used as

positive controls on every assay plate (see Table 2S for details). Compounds were assayed at final concentration of 50 μM ($n$ = 3).

**Crystallization, Preparation of the Inhibitor Complexes, and Data Collection** was performed by Proteros Biostructures GmbH, Martinsread, Germany**.**

*Protein Production.* Suitable constructs for GyrB expression had been previously established and expression of GyrB was performed according to previously established protocols. A purification protocol was established and homogeneous protein was produced in preparative amounts. The protein was purified comprising affinity and gel filtration chromatography steps. This procedure yielded homogenous protein with a purity greater 95% as judged from Coomassie stained SDS-PAGE.

*Crystallization.* The purified protein was used in crystallization trials employing both, a standard screen with approximately 1800 different conditions, as well as crystallization conditions identified using literature data. Conditions initially obtained have been optimized using standard strategies, systematically varying parameters critically influencing crystallization, such as temperature, protein concentration, drop ratio, and others. These conditions were also refined by systematically varying pH or precipitant concentrations.

*Data Collection and Processing.* A cryo-protocol was established using PROTEROS Standard Protocols. Crystals have been flash-frozen and measured at a temperature of 100 K. The X-ray diffraction data have been collected from complex crystals of GyrB with the ligand **18a** at the SWISS LIGHT SOURCE (SLS, Villigen, Switzerland) using cryogenic conditions. The crystals belong to space group C 2. Data were processed using the programs XDS and XSCALE. The data collection and refinement statistics are summarized in Tables 4 and 5.

**Table 4.** Data collection and processing statistics for **18a**.

| **Ligand** | **18a** |
|---|---|
| X-ray source | PXI/X06SA (SLS[a]) |
| Wavelength [Å] | 1.00000 |
| Detector | PILATUS 6M |
| Temperature [K] | 100 |

| | |
|---|---|
| Space group | C 2 |
| Cell: a; b; c; [Å] | 117.88; 50.55; 71.34 |
| α; β; γ; [◦] | 90.0; 93.5; 90.0 |
| Resolution [Å] | 2.20 (2.45-2.20)[b] |
| Unique reflections | 20677 (5706) |
| Multiplicity | 2.6 (2.6) |
| Completeness [%] | 95.9 (96.8) |
| $R_{sym}$ [%] | 4.5 (43.5) |
| $R_{meas}$ [%] | 5.5 (53.3) |
| Mean(I)/sd[c] | 13.86 (2.23) |

[a] SWISS LIGHT SOURCE (SLS, Villigen, Switzerland).
[b] Values in parenthesis refer to the highest resolution bin.
[c] Calculated from independent reflections.

**Table 5.** Refinement statistics for **18a**.[a]

| **Ligand** | **18a** |
|---|---|
| Resolution [Å] | 71.21-2.20 |
| Number of reflections (working/test) | 19273/1403 |
| $R_{cryst}$ [%] | 22.4 |
| $R_{free}$ [%][b] | 28.2 |
| Total number of atoms: | |
| Protein | 2784 |
| Water | 76 |
| Ligand | 23 |
| Iodide | 2 |
| Deviation from ideal geometry:[c] | |
| Bond lengths [Å] | 0.007 |
| Bond angles [°] | 1.10 |
| Bonded B's [$Å^2$][d] | 2.9 |
| Ramachandran plot:[e] | |
| Most favored regions [%] | 91.0 |
| Additional allowed regions [%] | 8.3 |
| Generously allowed regions [%] | 0.0 |
| Disallowed regions [%] | 0.6 |

[a] Values as defined in REFMAC5, without sigma cut-off.
[b] Test-set contains 6.8% of measured reflections.
[c] Root mean square deviations from geometric target values.
[d] Calculated with MOLEMAN.
[e] Calculated with PROCHECK.

**Molecular Modeling.** *Computer Hardware.* All of the computations were performed on a workstation with four eight-core AMD Opteron 6128 Magny-Cours 2.0 GHz processors, and 32 GB RAM, two 1 TB hard drives, and a 256 GB solid-state drive, running 64-bit Scientific Linux, release 6.2.

*Molecular Docking.* The three-dimensional model of compound **18a** was built in ChemBio3D Ultra 13.0.[34] The geometries of the molecules were optimized using MMFF94[35] force field and partial atomic charges. The energy was minimized until the gradient value was

smaller than 0.001 kcal/(mol Å). The optimized structure was further refined with GAMESS interface in ChemBio3D Ultra 13.0 using semiempirical PM3 method, QA optimization algorithm and Gasteiger Hückel charges for all atoms for 100 steps.[34] A library of 164 conformers of **18a** was then generated by OMEGA 2.4.6. (OpenEye Scientific Software, Inc., Santa Fe, NM, USA; www.eyesopen.com).[36,37] MAKE RECEPTOR 3.0.1 software (OpenEye Scientific Software, Inc., Santa Fe, NM, USA; www.eyesopen.com) was used for the protein preparation. A box of 4408 Å$^3$ was generated around the inhibitor from the crystal structure of *E. coli* GyrB (PDB entry: 4DUH[10]). After molecular cavity detection algorithm for site detection was used, a high-quality site shape potential of the final docking volume of 886 Å$^3$ was calculated. Of note, protonation state of the binding site residues and their conformations were not modified, and no constraints were used. The OMEGA-generated library of **18a** conformers was docked into the prepared enzyme binding site using FRED 3.0.1 software (OpenEye Scientific Software, Inc., Santa Fe, NM, USA; www.eyesopen.com) and the Chemgauss4 scoring function.[26,27] The best scored docking conformation was visualized by PyMOL.[25]

*Homology Modeling.* Completeness of the GyrB43-**18a** complex was improved by creating a homology model based on homologous *E. coli* topoisomerase IV ParE subunit (PDB entry: 4HZ0[17a]). Sequence alignment was performed using the T-COFFEE server[29] and the obtained alignment was used as input for homology modeling software MODELLER 9.13[28] to model the missing and incomplete residues. Ten models were generated and the best model for further studies was selected based on DOPE score and stereochemical quality of the model as evaluated by PROCHECK[30] and ProSA-web[31] server.

*Molecular Dynamics.* The molecular dynamics package NAMD (version 2.9)[38] and CHARMM22 force field[39] were used for molecular dynamics simulations of GyrB43-**18a** complex. Molecular mechanics parameters for compound **18a** were estimated using

ParamChem tool.[40] Steepest descent (10,000 steps) and adopted basis Newton–Raphson (10,000 steps) energy minimizations were first performed to remove atomic clashes and to optimize the atomic coordinates of the GyrB43-**18a** complex. The structure of the energy minimized complex for MD simulation was prepared using *psfgen* in VMD (version 1.9.1.).[41] The complex was then embedded in a box of water, which was modeled explicitly by a TIP3P model.[42] The system was neutralized by addition of KCl at 0.4 M concentration. The MD simulation was carried out in the NPT ensemble employing periodic boundary conditions. Langevin dynamics and Langevin piston methods were used for temperature (300 K) and pressure (1 atm) control, respectively. Short- and long-range forces were calculated every 1 and 2 time steps, respectively, with a time step of 2.0 ps. The smooth particle mesh Ewald method[43] was used to calculate electrostatic interactions. The short-range interactions were cut off at 12 Å. All chemical bonds between hydrogen and heavy atoms were held fixed using SHAKE algorithm.[44] The simulation consisted of three consecutive steps: (*i*) solvent equilibration for 1 ns with ligand and protein constrained harmonically around the initial structure, (*ii*) equilibration of the complete system for 1 ns with ligand and protein released, and (*iii*) an unconstrained 10 ns production run to allow the protein and the ligand to position themselves according to physical forces between them. The trajectory of the equilibration and production run was used for analysis in VMD. Distances between atoms (Figure 2S) were measured using the distance tool in VMD, data exported and analyzed in MS Excel.

**General Procedures - Chemistry.** Chemicals were obtained from Acros Organics (Geel, Belgium), Sigma-Aldrich (St. Louis, MO, USA) and Apollo Scientific (Stockport, UK) and used without further purification. Analytical TLC was performed on silica gel Merck 60 $F_{254}$ plates (0.25 mm), using visualization with UV light and spray reagents. Column chromatography was carried out on silica gel 60 (particle size 240–400 mesh). HPLC analyses were performed on an Agilent Technologies 1100 instrument (Agilent Technologies, Santa

Clara, CA, USA) with a G1365B UV-Vis detector, a G1316A thermostat and a G1313A autosampler using a Phenomenex Luna 5-μm C18 column (4.6 × 150 mm or 4.6 × 250 mm, Phenomenex, Torrance, CA, USA) and a flow rate of 1.0 mL/min. The eluent consisted of trifluoroacetic acid (0.1% in water) as solvent A and methanol or acetonitrile as solvent B. Melting points were determined on a Reichert hot stage microscope and are uncorrected. $^{1}$H and $^{13}$C NMR spectra were recorded at 400 and 100 MHz, respectively, on a Bruker AVANCE III 400 spectrometer (Bruker Corporation, Billerica, MA, USA) in DMSO-$d_6$ or $CDCl_3$ solutions, with TMS as the internal standard. IR spectra were recorded on a PerkinElmer Spectrum BX FT-IR spectrometer (PerkionElmer, Inc., Waltham, MA, USA) or Thermo Nicolet Nexus 470 ESP FT-IR spectrometer (Thermo Fisher Scientific, Waltham, MA, USA). Mass spectra were obtained using a VG Analytical Autospec Q mass spectrometer (Fisons, VG Analytical, Manchester, UK). Optical rotations were measured on a Perkin-Elmer 241 MC polarimeter. The reported values for specific rotation are average values of 10 successive measurements using an integration time of 5 s. The purity of the tested compounds was established to be ≥95%.

**Synthetic procedures.**

**General Procedure A. Synthesis of Compounds 15a-b (with 15a as an Example).** To a suspension of glycine methyl ester hydrochloride (**14a**) (1.35 g, 10.78 mmol) and potassium carbonate (4.47 g, 32.33 mmol) in acetonitrile (40 mL) cooled on an ice bath, a solution of 4-nitrobenzoyl chloride (**13**) (2.00 g, 10.78 mmol) in acetonitrile (10 mL) was added dropwise. The mixture was stirred at rt for 15 h upon which the solvent was evaporated under reduced pressure, the residue dissolved in ethyl acetate (50 mL) and washed successively with water (2 × 20 mL) and brine (2 × 15 mL). The organic phase was dried over $Na_2SO_4$, filtered and the solvent evaporated under reduced pressure to afford **15a** (1.91 g) as white crystals.

**Methyl (4-nitrobenzoyl)glycinate (15a).** White crystals; yield 74% (1.91 g); mp 150–152 °C (157–158 °C, lit[45]); IR (KBr) $\nu$ = 3295, 3104, 3009, 2953, 1740, 1655, 1599, 1547, 1518, 1490, 1432, 1346, 1329, 1308, 1257, 1204, 1166, 1107, 1013, 961, 875, 860, 822, 728 $cm^{-1}$. $^1H$ NMR (400 MHz, $CDCl_3$) $\delta$ 3.84 (s, 3H, $CH_3$), 4.28 (d, 2H, $^3J$ = 4.8 Hz, $CH_2$), 6.89 (br s, 1H, NH), 8.00 (d, 2H, $^3J$ = 8.4 Hz, Ar-H-2,6), 8.31 (d, 2H, $^3J$ = 8.4 Hz, Ar-H-3,5); $^{13}C$ NMR (100 MHz, $CDCl_3$) $\delta$ 41.87 ($CH_2$), 52.74 ($CH_3$), 123.90, 128.35, 139.15, 149.80, 165.45 (C=O), 170.20 (C=O).

**General Procedure B. Synthesis of Compounds 16a-b (with 16a as an Example).** Compound **15a** (1.85 g, 7.75 mmol) was dissolved in methanol (50 mL), Pd/C (500 mg) was added and the reaction mixture was stirred under hydrogen atmosphere for 5 h. The catalyst was filtered off and the solvent removed under reduced pressure to give **16a** (1.60 g) as a brown solid.

**Methyl (4-aminobenzoyl)glycinate (16a).**[46] Brown solid; yield 99% (1.60 g); mp 116–119 °C; IR (KBr) $\nu$ = 3442, 3351, 3240, 3037, 2954, 1750, 1634, 1600, 1500, 1439, 1409, 1366, 1298, 1203, 1177, 1001, 981, 837, 767 $cm^{-1}$. $^1H$ NMR (400 MHz, $CDCl_3$) $\delta$ 3.81 (s, 3H, $CH_3$), 4.03 (br s, 2H, $NH_2$), 4.24 (d, 1H, $^3J$ = 5.2 Hz, $CH_2$), 6.54 (br s, 1H, NH), 6.68 (d, 2H, $^3J$ = 8.4 Hz, Ar-H-3,5), 7.67 (d, 2H, $^3J$ = 8.4 Hz, Ar-H-2,6).

**General Procedure C. Synthesis of Compounds 17a-d (with 17a as an Example).** To a suspension of 4,5-dibromo-pyrrole-2-carboxylic acid (244 mg, 0.91 mmol) and TBTU (333 mg, 1.04 mmol) in dichloromethane (10 mL) *N*-methylmorpholine (0.285 mL, 2.59 mmol) was added, and the mixture stirred at rt for 0.5 h upon which a clear solution formed. Compound **16a** (180 mg, 0.86 mmol) was added and the mixture stirred at 50 °C for 15 h. The solvent was evaporated under reduced pressure, the residue dissolved in ethyl acetate (30 mL), and washed successively with water (2 × 15 mL) and brine (2 × 10 mL). The organic phase was dried over $Na_2SO_4$, filtered and the solvent evaporated under reduced pressure. To

the residue ether (10 mL) was added, the obtained suspension was sonicated, filtered, washed with ether (2 × 5 mL) and methanol (2 × 5 mL), and dried to afford **17a** (200 mg) as an off-white solid.

**Methyl (4-(4,5-dibromo-1*H*-pyrrole-2-carboxamido)benzoyl)glycinate (17a).** White solid; yield 50% (200 mg); mp 245–249 °C; IR (KBr) $\nu$ = 3608, 3385, 3287, 3118, 2952, 1728, 1655, 1632, 1599, 1528, 1495, 1414, 1372, 1344, 1317, 1249, 1218, 1184, 1161, 1122, 1068, 974, 849, 766, 736 $cm^{-1}$. $^1H$ NMR (400 MHz, DMSO-$d_6$) $\delta$ 3.66 (s, 3H, $CH_3$), 4.01 (d, 2H, $^3J$ = 6.0 Hz, $CH_2$), 7.28 (d, 1H, $^4J$ = 2.4 Hz, Pyrr-CH), 7.81–7.89 (m, 4H, AB-system, 4 × Ar-H), 8.87 (t, 1H, $^3J$ = 6.0 Hz, N<u>H</u>$CH_2$), 10.07 (s, 1H, NHAr), 12.99 (s, 1H, Pyrr-NH); $^{13}C$ NMR (100 MHz, DMSO-$d_6$) $\delta$ 41.17 ($CH_2$), 51.71 ($CH_3$), 98.25, 106.44, 114.21, 119.01, 127.63, 128.10, 128.17, 141.76, 157.42 (C=O), 166.04 (C=O), 170.48 (C=O); MS (ESI) $m/z$ (%) = 459.9 (50), 457.9 (100), 455.9 ($[M-H]^-$, 40). HRMS for $C_{15}H_{12}Br_2N_3O_4$: calculated 455.9195; found 455.9190. HPLC: Phenomenex Luna 5 μm C18 column (4.6 mm × 150 mm); mobile phase: 10–90% of MeOH in TFA (0.1%) in 20 min, 90% MeOH to 25 min; flow rate 1.0 mL/min; injection volume: 10 μL; retention time: 18.549 min (96.6% at 280 nm).

**General Procedure D. Synthesis of Compounds 18a-d (with 18a as an Example).** To a stirred solution of **17a** (118 mg, 0.257 mmol) in THF/water (2:1, 10 mL), 2 M LiOH (0.193 mL, 0.386 mmol) was added. The mixture was stirred at rt for 5 h, neutralized with 1 M HCl and concentrated under reduced pressure. The residual aqueous solution was acidified to pH 2 with 1 M HCl and the product extracted with ethyl acetate (3 × 15 mL). The combined organic phases were washed with water (2 × 15 mL) and brine (2 × 10 mL), dried over $Na_2SO_4$, filtered and the solvent evaporated under reduced pressure. To the residue ether (10 mL) was added, the obtained suspension was sonicated, filtered, washed with ether (2 × 5 mL) and dried to afford **18a** (102 mg) as an off-white solid.

**(4-(4,5-Dibromo-1*H*-pyrrole-2-carboxamido)benzoyl)glycine (18a).** Off-white solid; yield 89% (102 mg); mp 250–254 °C; IR (KBr) $\nu$ = 3340, 3138, 3104, 2955, 1721, 1653, 1607, 1589, 1522, 1504, 1445, 1406, 1384, 1335, 1309, 1238, 1205, 1189, 1107, 1018, 1001, 974, 871, 851, 834, 821, 764 $cm^{-1}$. $^1H$ NMR (400 MHz, DMSO-$d_6$) $\delta$ 3.92 (d, 2H, $^3J$ = 6.0 Hz, $CH_2$), 7.28 (s, 1H, Pyrr-CH), 7.80–7.80 (m, 4H, AB-system, 4 × Ar-H), 8.75 (t, 1H, $^3J$ = 6.0 Hz, N<u>H</u>$CH_2$), 10.06 (s, 1H, NHAr), 12.60 (s, 1H, COOH/Pyrr-NH), 12.98 (s, 1H, COOH/Pyrr-NH); $^{13}C$ NMR (100 MHz, DMSO-$d_6$) $\delta$ 41.15 ($CH_2$), 98.25, 106.41, 114.20, 119.00, 127.64, 128.06, 128.42, 141.65, 157.41 (C=O), 166.92 (C=O), 171.42 (C=O); MS (ESI) *m*/*z* (%) = 445.9 (50), 443.9 (100), 441.9 ([M-H]$^-$, 40). HRMS for $C_{14}H_{10}Br_2N_3O_4$: calculated 441.9038; found 441.9049. HPLC: Phenomenex Luna 5 μm C18 column (4.6 mm × 150 mm); mobile phase: 10–90% of MeOH in TFA (0.1%) in 20 min, 90% MeOH to 25 min; flow rate 1.0 mL/min; injection volume: 10 μL; retention time: 17.840 min (98.5% at 280 nm).

**General Procedure E. Synthesis of Compounds 19a-c (with 19a as an Example).** A solution of **18a** (21 mg, 0.046 mmol) in MeOH/THF (5:1, 6 mL) was cooled on an ice bath, saturated with gaseous $NH_3$ and stirred at rt for 15 h. The solvent was removed under reduced pressure, to the residue ether (5 mL) was added, the obtained suspension was sonicated, filtered, washed with ether (2 × 2 mL) and dried to afford **19a** (14 mg) as a white solid.

***N*-(4-((2-Amino-2-oxoethyl)carbamoyl)phenyl)-4,5-dibromo-1*H*-pyrrole-2-carboxamide (19a).** White solid; yield 68% (14 mg); mp 285–289 °C; IR (KBr) $\nu$ = 3463, 3323, 3177, 3105, 2970, 1677, 1662, 1636, 1593, 1515, 1411, 1332, 1299, 1249, 1233, 1187, 1110, 995, 971, 835, 763 $cm^{-1}$. $^1H$ NMR (400 MHz, DMSO-$d_6$) $\delta$ 3.81 (d, 2H, $^3J$ = 5.6 Hz, $CH_2$), 7.05 (s, 1H, $H_A$ from $NH_2$), 7.27 (s, 1H, Pyrr-CH), 7.37 (s, 1H, $H_B$ from $NH_2$), 7.79–7.89 (m, 4H, AB-system, 4 × Ar-H), 8.57 (t, 1H, $^3J$ = 5.6 Hz, N<u>H</u>$CH_2$), 10.04 (s, 1H, NHAr), 12.97 (s, 1H, Pyrr-NH); $^{13}C$ NMR (100 MHz, DMSO-$d_6$) $\delta$ 42.33 ($CH_2$), 98.24, 106.41, 114.16, 118.92,

127.66, 128.14, 128.70, 141.52, 157.42 (C=O), 165.85 (C=O), 171.13 (C=O); MS (ESI) *m*/*z* (%) = 444.9 (49), 442.9 (100), 440.9 ([M-H]$^-$, 50). HRMS for $C_{14}H_{11}Br_2N_4O_3$: calculated 440.9198; found 440.9193. HPLC: Phenomenex Luna 5 μm C18 column (4.6 mm × 150 mm); mobile phase: 30–90% of acetonitrile in TFA (0.1%) in 16 min, 90% acetonitrile to 20 min; flow rate 1.0 mL/min; injection volume: 10 μL; retention time: 6.039 min (99.1% at 280 nm).

**General Procedure F. Synthesis of Compounds 22a-b (with 22a as an Example).** A suspension of 4-nitrophenol (**20a**, 1.50 g, 10.8 mmol), methyl 2-bromoacetate (**21**, 1.02 mL, 11.8 mmol) and potassium carbonate (2.98 g, 21.6 mmol) in acetonitrile (50 mL) was stirred at rt for 15 h. The solvent was removed under reduced pressure, the residue dissolved in ethyl acetate (50 mL), washed with water (2 × 20 mL) and brine (2 × 15 mL), dried over $Na_2SO_4$ and concentrated under reduced pressure to afford **22a** (2.12 g, 10.0) as a white solid.

**Methyl 2-(4-nitrophenoxy)acetate (22a).** White solid; yield 93% (2.12 g); mp 98–100 °C (98–99 °C, lit[47]); IR (KBr) *v* = 3402, 3313, 3116, 2956, 1756, 1722, 1610, 1592, 1498, 1436, 1330, 1198, 1173, 1110, 1000, 856, 752 cm$^{-1}$. $^1$H NMR (400 MHz, DMSO-$d_6$) $\delta$ 3.72 (s, 3H, $CH_3$), 5.02 (s, 2H, $CH_2$), 7.12 (d, 2H, $^3J$ = 9.2 Hz, Ar-H-2,6), 8.21 (d, 2H, $^3J$ = 9.2 Hz, Ar-H-3,5).

**Methyl 2-(4-aminophenoxy)acetate (23a).** Synthesized according to General procedure B in THF/MeOH (1:1, 50 mL) as solvent. Brown solid; yield 98% (1.73 g); mp 215–217 °C; IR (KBr) *v* = 3456, 3434, 3359, 3046, 2953, 2922, 2856, 1748, 1509, 1440, 1214, 826 cm$^{-1}$. $^1$H NMR (400 MHz, DMSO-$d_6$) $\delta$ 3.68 (s, 3H, $CH_3$), 4.60 (s, 2H, $CH_2$), 4.68 (s, 2H, $NH_2$), 6.50 (d, 2H, $^3J$ = 9.2 Hz, Ar-H-2,6), 6.65 (d, 2H, $^3J$ = 9.2 Hz, Ar-H-3,5).

**Methyl 2-(4-(4,5-dibromo-1*H*-pyrrole-2-carboxamido)phenoxy)acetate (24a).** Synthesized according to General procedure C. Brown solid; yield 46% (165 mg); mp 190–192 °C; IR (KBr) *v* = 3388, 3300, 3204, 2955, 2852, 1757, 1730, 1650, 1553, 1525, 1509, 1417, 1389, 1223, 1177, 1078, 973, 820, 750 cm$^{-1}$. $^1$H NMR (400 MHz, DMSO-$d_6$) $\delta$ 3.71 (s, 3H, $CH_3$),

4.78 (s, 2H, $CH_2$), 6.93 (d, 2H, $^3J$ = 9.2 Hz, Ar-H-2,6), 7.19 (s, 1H, Pyrr-CH), 7.60 (d, 2H, $^3J$ = 9.2 Hz, Ar-H-3,5), 9.77 (s, 1H, NH), 12.88 (s, 1H, Pyrr-NH). $^{13}$C NMR (100 MHz, DMSO-$d_6$) $\delta$ 51.77 ($CH_3$), 64.71 ($CH_2$), 64.90, 98.03, 105.55, 113.44, 114.55, 121.49, 127.97, 132.38, 153.67, 157.07, 169.29; MS (ESI) *m*/*z* (%) = 428.9 ([M-H]$^-$). HRMS for $C_{14}H_{11}Br_2N_2O_4$: calculated 428.9086; found 428.9088. HPLC: Phenomenex Luna 5 μm C18 column (4.6 mm × 150 mm); mobile phase: 10–90% of MeOH in TFA (0.1%) in 20 min, 90% MeOH to 25 min; flow rate 1.0 mL/min; injection volume: 10 μL; retention time: 19.554 min (98.6% at 280 nm).

**2-(4-(4,5-Dibromo-1*H*-pyrrole-2-carboxamido)phenoxy)acetic acid (25a).** Synthesized according to General procedure D in MeOH/water (5:1, 20 mL) as solvent. Brown solid; yield 93% (90 mg); mp 242–244 °C; IR (KBr) *v* = 3408, 3139, 3108, 2936, 2538, 1708, 1626, 1600, 1514, 1417, 1311, 1250, 1208, 1174, 1074, 975, 820, 803, 754 cm$^{-1}$. $^1$H NMR (400 MHz, DMSO-$d_6$) $\delta$ 4.65 (s, 2H, $CH_2$), 6.91 (d, 2H, $^3J$ = 9.2 Hz, Ar-H-2,6), 7.19 (d, 1H, $^4J$ = 2.4 Hz, Pyrr-CH), 7.59 (d, 2H, $^3J$ = 9.2 Hz, Ar-H-3,5), 9.77 (s, 1H, NH), 12.88 (d, 1H, $^4J$ = 2.4 Hz, Pyrr-NH), 12.99 (br s, 1H, COOH). $^{13}$C NMR (100 MHz, DMSO-$d_6$) $\delta$ 64.60 ($CH_2$), 98.02, 105.51, 113.42, 114.45, 121.49, 128.00, 132.17, 153.85, 157.05, 170.25; MS (ESI) *m*/*z* (%) = 414.9 ([M-H]$^-$). HRMS for $C_{13}H_9Br_2N_2O_4$: calculated 414.8929; found 414.8921. HPLC: Phenomenex Luna 5 μm C18 column (4.6 mm × 150 mm); mobile phase: 10–90% of MeOH in TFA (0.1%) in 20 min, 90% MeOH to 25 min; flow rate 1.0 mL/min; injection volume: 10 μL; retention time: 18.676 min (98.6% at 280 nm).

***N*,*N*-Dimethyl-2-(4-nitrophenoxy)ethan-1-amine (27a).**[48] A suspension of 4-nitrophenol (**50a**, 0.500 g, 3.59 mmol), 2-chloro-*N*,*N*-dimethylethylamine hydrochloride (**26a**, 0.621 g, 4.31 mmol) and potassium carbonate (1.49 g, 10.78 mmol) in acetonitrile (10 mL) was heated at 50 °C for 15 h. The solvent was removed under reduced pressure, the residue dissolved in ethyl acetate (30 mL), washed with water (2 × 10 mL), saturated aqueous $NaHCO_3$ solution (2

× 10 mL) and brine (2 × 10 mL), dried over $Na_2SO_4$ and concentrated under reduced pressure. The crude product was purified with flash column chromatography using ethyl acetate as an eluent to afford **27a** (127 mg) as a yellow oil. Yield 17% (127 mg); IR (KBr) $\nu$ = 3114, 3080, 2946, 2825, 2777, 1668, 1591, 1506, 1468, 1334, 1278, 1256, 1173, 1109, 1025, 959, 909, 845, 751 $cm^{-1}$. $^1H$ NMR (400 MHz, DMSO-$d_6$) $\delta$ 2.22 (s, 6H, 2 × $CH_3$), 2.66 (t, 2H, $^3J$ = 5.6 Hz, $CH_2N$), 4.21 (t, 2H, $^3J$ = 5.6 Hz, $OCH_2$), 7.17 (d, 2H, $^3J$ = 9.6 Hz, Ar-H-2,6), 8.21 (d, 2H, $^3J$ = 9.6 Hz, Ar-H-3,5); $^{13}C$ NMR (100 MHz, $CDCl_3$) $\delta$ 45.84 (2 × $CH_3$), 57.90 ($CH_2N$), 66.72 ($OCH_2$), 114.54, 125.91, 141.55, 163.82.

**4-(2-(Dimethylamino)ethoxy)aniline (28a).**[49] Synthesized according to General procedure B with ethanol as solvent. Brown oil; yield 90% (83 mg); IR (KBr) $\nu$ = 3339, 3216, 2943, 2869, 2823, 2775, 1628, 1508, 1463, 1408, 1367, 1228, 1190, 1171, 1097, 1031, 959, 910, 823, 722 $cm^{-1}$. $^1H$ NMR (400 MHz, $CDCl_3$) $\delta$ 2.36 (s, 6H, 2 × $CH_3$), 2.73 (t, 2H, $^3J$ = 5.6 Hz, $CH_2N$), 3.19 (br s, 2H, $NH_2$), 4.02 (t, 2H, $^3J$ = 5.6 Hz, $OCH_2$), 6.65 (d, 2H, $^3J$ = 8.8 Hz, 2 × Ar-H), 6.78 (d, 2H, $^3J$ = 8.8 Hz, 2 × Ar-H); $^{13}C$ NMR (100 MHz, $CDCl_3$) $\delta$ 45.85 (2 × $CH_3$), 58.40 ($CH_2N$), 66.52 ($OCH_2$), 115.75, 116.37, 140.09, 151.98.

**4,5-Dibromo-*N*-(4-(2-(dimethylamino)ethoxy)phenyl)-1*H*-pyrrole-2-carboxamide (29a).** To a suspension of 4,5-dibromo-pyrrole-2-carboxylic acid (121 mg, 0.45 mmol) and TBTU (158 mg, 0.49 mmol) in dichloromethane (5 mL) *N*-methylmorpholine (0.135 mL, 1.23 mmol) was added, and the mixture stirred at rt for 0.5 h upon which a clear solution formed. Compound **28a** (74 mg, 0.41 mmol) was added and the mixture stirred at 50 °C for 15 h. The solvent was evaporated under reduced pressure, and to the residue ethyl acetate (5 mL) and water (5 mL) were added. The undissolved precipitate was filtered off, washed with ethyl acetate (2 × 2 mL) and dried. The obtained solid was treated with methanol, the precipitate was filtered off and the filtrate evaporated under reduced pressure. To the residue after evaporation ether (5 mL) was added, and the obtained suspension was sonicated, filtered,

washed with ether (2 × 2 mL) and dried to afford **29a** as a white solid (101 mg). Yield 57% (101 mg); mp 142–145 °C; IR (KBr) $\nu$ = 3048, 2950, 2787, 2692, 1642, 1604, 1559, 1511, 1467, 1415, 1385, 1328, 1297, 1229, 1176, 1124, 1046, 1027, 958, 973, 909, 858, 826, 790 $cm^{-1}$. $^1H$ NMR (400 MHz, DMSO-$d_6$) $\delta$ 2.25 (s, 6H, 2 × $CH_3$), 2.66 (t, 2H, $^3J$ = 5.6 Hz, $CH_2N$), 4.04 (t, 2H, $^3J$ = 5.6 Hz, $OCH_2$), 6.93 (d, 2H, $^3J$ = 9.2 Hz, 2 × Ar-H), 7.17 (s, 1H, Pyrr-CH), 7.59 (d, 2H, $^3J$ = 8.8 Hz, 2 × Ar-H), 9.73 (s, 1H, CONH), 12.79 (br s, 1H, Pyrr-NH); $^{13}C$ NMR (100 MHz, DMSO-$d_6$) $\delta$ 45.92 (2 × $CH_3$), 58.10 ($CH_2N$), 66.20 ($OCH_2$), 98.39, 106.16, 113.87, 114.94, 121.99, 128.68, 132.33, 155.04, 157.64; MS (ESI) $m/z$ (%) = 431.9 (50), 429.9 (100), 427.9 ($[M-H]^-$, 50). HRMS for $C_{15}H_{16}Br_2N_3O_2$: calculated 427.9609; found 427.9619. HPLC: Phenomenex Luna 5 μm C18 column (4.6 mm × 150 mm); mobile phase: 10–90% of MeOH in TFA (0.1%) in 20 min, 90% MeOH to 25 min; flow rate 1.0 mL/min; injection volume: 10 μL; retention time: 16.514 min (98.2% at 280 nm).

**Methyl 4-nitrobenzimidate hydrochloride (31).** A solution of 4-nitrobenzonitrile (**30**, 0.500 g, 3.38 mmol) in a mixture of methyl acetate (20 mL) and methanol (2 mL) was cooled on an ice-bath, saturated with gaseous HCl and stirred at 4 °C for 48 h. The solvent was evaporated under reduced pressure, to the solid residue ether (10 mL) was added, the obtained suspension was sonicated, filtered, washed with ether (2 × 5 mL) and dried to afford **31** (0.540 g, 2.49 mmol, 74% yield) as a white solid. The crude product was used in the next step without further purification.

**Methyl (*S*)-2-(4-nitrophenyl)-4,5-dihydrooxazole-4-carboxylate (32).**[50] To a solution of compound **31** (200 mg, 0.923 mmol) in dichloromethane (50 mL) triethylamine (148 μL, 1.06 mmol) was added and the mixture stirred for 30 min. L-Serine methyl ester hydrochloride (182 mg, 1.17 mmol) was added, the mixture stirred at rt for 48 h and the solvent evaporated under reduced pressure. The crude product was purified with flash column chromatography using ethyl acetate/petroleum ether (2:1) as an eluent, to give **32** (204 mg, 0.816 mmol) as an

off-white solid. Yield 88% (204 mg); mp 105–107 °C; $[\alpha]_D$ +70.8 (*c* 0.209, MeOH); IR (KBr) *v* = 3399, 3319, 3110, 2957, 1751, 1651, 1598, 1519, 1409, 1340, 1310, 1210, 1065, 1010, 956, 937, 860, 852, 697 $cm^{-1}$. $^1H$ NMR (400 MHz, DMSO-$d_6$) $\delta$ 3.73 (s, 3H, $CH_3$), 4.64–4.73 (m, 2H, $CH_2$), 5.07 (dd, 1H, $^3J_1$ = 10.0 Hz, $^3J_2$ = 8.0 Hz, CH), 8.14 (d, 1H, $^3J$ = 8.8 Hz, Ar-H-2,6), 8.34 (d, 1H, $^3J$ = 8.8 Hz, Ar-H-3,5); $^{13}C$ NMR (100 MHz, DMSO-$d_6$) $\delta$ 52.36 ($CH_3$), 68.26 (CH/$CH_2$), 70.30 (CH/$CH_2$), 123.95, 129.47, 132.21, 149.43, 163.32, 171.02.

**Methyl (*S*)-2-(4-aminophenyl)-4,5-dihydrooxazole-4-carboxylate (33).** Synthesized according to General Procedure B, with ethanol (20 mL) as solvent. Orange solid; yield 94% (145 mg); mp 120–123 °C; $[\alpha]_D$ +111.1 (*c* 0.149, MeOH); IR (KBr) *v* = 3494, 3391, 3348, 1724, 1606, 1518, 1359, 1213, 1174, 1092, 974 $cm^{-1}$. $^1H$ NMR (400 MHz, DMSO-$d_6$) $\delta$ 3.69 (s, 3H, $CH_3$), 4.44–4.52 (m, 2H, $CH_2$), 4.83 (dd, 1H, $^3J_1$ = 10.0 Hz, $^3J_2$ = 7.6 Hz, CH), 5.83 (s, 2H, $NH_2$), 6.56 (d, 1H, $^3J$ = 8.8 Hz, Ar-H-3,5), 7.54 (d, 1H, $^3J$ = 8.8 Hz, Ar-H-2,6); $^{13}C$ NMR (100 MHz, DMSO-$d_6$) $\delta$ 52.08 ($CH_3$), 67.82 (CH/$CH_2$), 68.99 (CH/$CH_2$), 112.85, 112.99, 129.61, 152.25, 165.21, 171.97. MS (ESI) *m*/*z* (%) = 221.1 ($MH^+$). HRMS for $C_{11}H_{13}N_2O_3$: calculated 221.0926; found 221.0922.

**Methyl (*S*)-2-(4-(4,5-dibromo-1*H*-pyrrole-2-carboxamido)phenyl)-4,5-dihydrooxazole-4-carboxylate (34).** Synthesized according to General Procedure C. To the solid residue after the extraction methanol (5 mL) was added, the obtained suspension was sonicated, filtered, washed with methanol (2 × 5 mL) and dried. Yellow solid; yield 38% (96 mg); mp 135–136 °C; $[\alpha]_D$ +19.9 (*c* 0.139, MeOH); IR (KBr) *v* = 3111, 3047, 2954, 2869, 1735, 1653, 1632, 1597, 1535, 1510, 1415, 1372, 1336, 1299, 1244, 1177, 1103, 972, 838, 740, 681 $cm^{-1}$. $^1H$ NMR (400 MHz, DMSO-$d_6$) $\delta$ 3.72 (s, 3H, $CH_3$), 4.54–4.63 (m, 2H, $CH_2$), 4.95 (dd, 1H, $^3J_1$ = 10.0 Hz, $^3J_2$ = 7.6 Hz, CH), 7.29 (d, 1H, $^3J$ = 2.4 Hz, Pyrr-CH), 7.84–7.89 (m, 4H, Ar-H-2,3,5,6), 10.10 (s, 1H, CONH), 12.99 (d, 1H, $^3J$ = 2.4 Hz, Pyrr-NH); $^{13}C$ NMR (100 MHz, DMSO-$d_6$) $\delta$ 52.22 ($CH_3$), 68.00 (CH/$CH_2$), 69.55 (CH/$CH_2$), 98.28, 106.54, 114.31, 119.27,

121.18, 127.57, 128.93, 142.19, 157.43, 164.45, 171.57. MS (ESI) *m*/*z* (%) = 467.9 ([M-H]$^-$). HRMS for $C_{16}H_{12}Br_2N_3O_4$: calculated 467.9195; found 467.9185. HPLC: Phenomenex Luna 5 μm C18 column (4.6 mm × 150 mm); mobile phase: 10–90% of MeOH in TFA (0.1%) in 20 min, 90% MeOH to 25 min; flow rate 1.0 mL/min; injection volume: 10 μL; retention time: 18.133 min (95.7% at 280 nm).

**(*S*)-2-(4-(4,5-Dibromo-1*H*-pyrrole-2-carboxamido)phenyl)-4,5-dihydrooxazole-4-carboxylic acid (35).** Synthesized according to General Procedure D, with methanol (10 mL) as solvent. Yellow solid; yield 55% (18 mg); mp 188–191 °C; $[\alpha]_D$ +13.5 (*c* 0.070, MeOH); IR (KBr) *v* = 3112, 2969, 1719, 1646, 1594, 1518, 1386, 1332, 1252, 1180, 1127, 973, 848, 744 cm$^{-1}$. $^1$H NMR (400 MHz, DMSO-$d_6$) $\delta$ 4.51–4.60 (m, 2H, $CH_2$), 4.84 (dd, 1H, $^3J_1$ = 9.6 Hz, $^3J_2$ = 8.0 Hz, CH), 7.29 (s, 1H, Pyrr-CH), 7.83–7.89 (m, 4H, Ar-H-2,3,5,6), 10.09 (s, 1H, CONH), 13.00 (br s, 2H, Pyrr-NH, COOH); $^{13}$C NMR (100 MHz, DMSO-$d_6$) $\delta$ 68.33 (CH/$CH_2$), 69.65 (CH/$CH_2$), 98.23, 106.60, 114.31, 119.26, 127.68, 128.84, 130.30, 142.06, 157.49, 163.93, 172.54. MS (ESI) *m*/*z* (%) = 453.9 ([M-H]$^-$). HRMS for $C_{15}H_{10}Br_2N_3O_4$: calculated 453.9038; found 453.9032. HPLC: Phenomenex Luna 5 μm C18 column (4.6 mm × 150 mm); mobile phase: 10–90% of MeOH in TFA (0.1%) in 20 min, 90% MeOH to 25 min; flow rate 1.0 mL/min; injection volume: 10 μL; retention time: 17.524 min (98.5% at 280 nm).

**Screening against PAINS**. To evaluate a library of the synthesized compounds against PAINS,[51] all tested compounds were screened against the PAINS filter using Python script filter_pains.py, downloaded from GitHub (https://github.com/Team-SKI/snippets/blob/1d1d0424ba15da08cdc7e18c9a27d55b1a6cb797/Python/filter_pains.py). All compounds passed the PAINS filter.

ASSOCIATED CONTENT

**Supporting Information.** Description of structure modeling and refinement, antibacterial activity of compounds, detailed experimental procedures, analytical data and NMR spectra. This material is available free of charge via the Internet at http://pubs.acs.org.

AUTHOR INFORMATION

**Corresponding Author**

*E-mail: danijel.kikelj@ffa.uni-lj.si. Phone: +386-1-4769561. Fax: +386-1-4258031.

**Author Contributions**

The manuscript was written through contributions of all authors. All authors have given approval to the final version of the manuscript.

**Funding Sources**

The work was founded by the Slovenian Research Agency (Grant No. P1-0208 and Grant No. Z1-5458) and by the EU FP7 Integrated Project MAREX (Project No. FP7-KBBE-2009-3-245137).

**Notes**

The authors declare no competing financial interest.

ACKNOWLEDGMENT

This work was supported by the Slovenian Research Agency (Grant No. P1-0208 and Grant No. Z1-5458) and by the EU FP7 Integrated Project MAREX (Project No. FP7-KBBE-2009-3-245137). We thank Dr. Dušan Žigon (Mass Spectrometry Center, Jožef Stefan Institute, Ljubljana, Slovenia) for recording mass spectra. We thank OpenEye Scientific Software, Santa Fe, NM., for free academic licenses for the use of their software.

ABBREVIATIONS

ATCC, American type culture collection; ATR, attenuated total reflectance; CFU, colony-forming unit; CLSI, Clinical and Laboratory Standards Institute; EDC, *N*-ethyl-*N*′-(3-dimethylaminopropyl)carbodiimide hydrochloride; GyrA, DNA gyrase A; GyrB, DNA gyrase B; $K_d$, dissociation constant; MH, Mueller Hinton; NHS, *N*-hydroxysuccinimide; NMM, *N*-methylmorpholine; ParC, topoisomerase IV subunit A; ParE, topoisomerase IV subunit B; RA, residual activity; SPR, surface plasmon resonance; TBTU, *N,N,N′,N′*-tetramethyl-*O*-(benzotriazol-1-yl)uronium tetrafluoroborate; topo IV, topoisomerase IV; VS, virtual screening.

REFERENCES

1. Lederberg, J., Infectious history. *Science* **2000**, *288* (5464), 287-293.

2. (a) Theuretzbacher, U., Accelerating resistance, inadequate antibacterial drug pipelines and international responses. *Int J Antimicrob Ag* **2012**, *39* (4), 295-299; (b) Silver, L. L., Challenges of antibacterial discovery. *Clin Microbiol Rev* **2011**, *24* (1), 71-109; (c) Payne, D. J.; Gwynn, M. N.; Holmes, D. J.; Pompliano, D. L., Drugs for bad bugs: confronting the challenges of antibacterial discovery. *Nat Rev Drug Discov* **2007**, *6* (1), 29-40.

3. (a) Mayer, C.; Janin, Y. L., Non-quinolone inhibitors of bacterial type IIA topoisomerases: a feat of bioisosterism. *Chem Rev* **2014**, *114* (4), 2313-2342; (b) Tomasic, T.; Masic, L. P., Prospects for developing new antibacterials targeting bacterial type IIA topoisomerases. *Curr Top Med Chem* **2014**, *14* (1), 130-151; (c) Oblak, M.; Kotnik, M.; Solmajer, T., Discovery and development of ATPase inhibitors of DNA gyrase as antibacterial agents. *Curr Med Chem* **2007**, *14* (19), 2033-2047.

4. Forterre, P.; Gribaldo, S.; Gadelle, D.; Serre, M. C., Origin and evolution of DNA topoisomerases. *Biochimie* **2007**, *89* (4), 427-446.

5. Champoux, J. J., DNA topoisomerases: structure, function, and mechanism. *Annu Rev Biochem* **2001**, *70*, 369-413.

6. Heide, L., New aminocoumarin antibiotics as gyrase inhibitors. *Int J Med Microbiol* **2014**, *304* (1), 31-36.

7. Konc, J.; Janežič, D., ProBiS-2012: web server and web services for detection of structurally similar binding sites in proteins. *Nucleic Acids Res* **2012**, *40* (W1), W214-W221.

8. Emmerson, A. M.; Jones, A. M., The quinolones: decades of development and use. *J Antimicrob Chemoth* **2003**, *51*, 13-20.

9. (a) Lafitte, D.; Lamour, V.; Tsvetkov, P. O.; Makarov, A. A.; Klich, M.; Deprez, P.; Moras, D.; Briand, C.; Gilli, R., DNA gyrase interaction with coumarin-based inhibitors: the role of the hydroxybenzoate isopentenyl moiety and the 5'-methyl group of the noviose. *Biochemistry-Us* **2002**, *41* (23), 7217-7223; (b) Holdgate, G. A.; Tunnicliffe, A.; Ward, W. H. J.; Weston, S. A.; Rosenbrock, G.; Barth, P. T.; Taylor, I. W. F.; Pauptit, R. A.; Timms, D., The entropic penalty of ordered water accounts for weaker binding of the antibiotic novobiocin to a resistant mutant of DNA gyrase: a thermodynamic and crystallographic study. *Biochemistry-Us* **1997**, *36* (32), 9663-9673; (c) Tsai, F. T. F.; Singh, O. M. P.; Skarzynski, T.; Wonacott, A. J.; Weston, S.; Tucker, A.; Pauptit, R. A.; Breeze, A. L.; Poyser, J. P.; OBrien, R.; Ladbury, J. E.; Wigley, D. B., The high-resolution crystal structure of a 24-kDa gyrase B fragment from *E. coli* complexed with one of the most potent coumarin inhibitors, clorobiocin. *Proteins* **1997**, *28* (1), 41-52; (d) Lewis, R. J.; Singh, O. M. P.; Smith, C. V.; Skarzynski, T.; Maxwell, A.; Wonacott, A. J.; Wigley, D. B., The nature of inhibition of DNA gyrase by the coumarins and the cyclothialidines revealed by X-ray crystallography. *Embo J* **1996**, *15* (6), 1412-1420.

10. Brvar, M.; Perdih, A.; Renko, M.; Anderluh, G.; Turk, D.; Solmajer, T., Structure-based discovery of substituted 4,5'-bithiazoles as novel DNA gyrase inhibitors. *J Med Chem* **2012**, *55* (14), 6413-6426.

11. (a) Oblak, M.; Grdadolnik, S. G.; Kotnik, M.; Jerala, R.; Filipič, M.; Solmajer, T., In silico fragment-based discovery of indolin-2-one analogues as potent DNA gyrase inhibitors. *Bioorg Med Chem Lett* **2005**, *15* (23), 5207-5210; (b) Oblak, M.; Grdadolnik, S. G.; Kotnik, M.; Poterszman, A.; Atkinson, R. A.; Nierengarten, H.; Desplancq, D.; Moras, D.; Solmajer, T., Biophysical characterization of an indolinone inhibitor in the ATP-binding site of DNA gyrase. *Biochem Bioph Res Co* **2006**, *349* (4), 1206-1213.

12. Lubbers, T.; Angehrn, P.; Gmunder, H.; Herzig, S., Design, synthesis, and structure-activity relationship studies of new phenolic DNA gyrase inhibitors. *Bioorg Med Chem Lett* **2007**, *17* (16), 4708-4714.

13. Starr, J. T.; Sciotti, R. J.; Hanna, D. L.; Huband, M. D.; Mullins, L. M.; Cai, H.; Gage, J. W.; Lockard, M.; Rauckhorst, M. R.; Owen, R. M.; Lall, M. S.; Tomilo, M.; Chen, H. F.; McCurdy, S. P.; Barbachyn, M. R., 5-(2-Pyrimidinyl)-imidazo[1,2-*a*]pyridines are antibacterial agents targeting the ATPase domains of DNA gyrase and topoisomerase IV. *Bioorg Med Chem Lett* **2009**, *19* (18), 5302-5306.

14. (a) Charifson, P. S.; Grillot, A. L.; Grossman, T. H.; Parsons, J. D.; Badia, M.; Bellon, S.; Deininger, D. D.; Drumm, J. E.; Gross, C. H.; LeTiran, A.; Liao, Y. S.; Mani, N.; Nicolau, D. P.; Perola, E.; Ronkin, S.; Shannon, D.; Swenson, L. L.; Tang, Q.; Tessier, P. R.; Tian, S. K.; Trudeau, M.; Wang, T. S.; Wei, Y. Y.; Zhang, H.; Stamos, D., Novel dual-targeting benzimidazole urea inhibitors of DNA gyrase and topoisomerase IV possessing potent antibacterial activity: intelligent design and evolution through the judicious use of structure-guided design and stucture-activity relationships. *J Med Chem* **2008**, *51* (17), 5243-5263; (b) Grossman, T. H.; Bartels, D. J.; Mullin, S.; Gross, C. H.; Parsons, J. D.; Liao, Y. S.; Grillot,

A. L.; Stamos, D.; Olson, E. R.; Charifson, P. S.; Mani, N., Dual targeting of GyrB and ParE by a novel aminobenzimidazole class of antibacterial compounds. *Antimicrob Agents Ch* **2007**, *51* (2), 657-666; (c) Mani, N.; Gross, C. H.; Parsons, J. D.; Hanzelka, B.; Muh, U.; Mullin, S.; Liao, Y. S.; Grillot, A. L.; Stamos, D.; Charifson, P. S.; Grossman, T. H., In vitro characterization of the antibacterial spectrum of novel bacterial type II topoisomerase inhibitors of the aminobenzimidazole class. *Antimicrob Agents Ch* **2006**, *50* (4), 1228-1237.

15. Ronkin, S. M.; Badia, M.; Bellon, S.; Grillot, A. L.; Gross, C. H.; Grossman, T. H.; Mani, N.; Parsons, J. D.; Stamos, D.; Trudeau, M.; Wei, Y. Y.; Charifson, P. S., Discovery of pyrazolthiazoles as novel and potent inhibitors of bacterial gyrase. *Bioorg Med Chem Lett* **2010**, *20* (9), 2828-2831.

16. Manchester, J. I.; Dussault, D. D.; Rose, J. A.; Boriack-Sjodin, P. A.; Uria-Nickelsen, M.; Ioannidis, G.; Bist, S.; Fleming, P.; Hull, K. G., Discovery of a novel azaindole class of antibacterial agents targeting the ATPase domains of DNA gyrase and topoisomerase IV. *Bioorg Med Chem Lett* **2012**, *22* (15), 5150-5156.

17. (a) Tari, L. W.; Trzoss, M.; Bensen, D. C.; Li, X. M.; Chen, Z. Y.; Lam, T.; Zhang, J. H.; Creighton, C. J.; Cunningham, M. L.; Kwan, B.; Stidham, M.; Shaw, K. J.; Lightstone, F. C.; Wong, S. E.; Nguyen, T. B.; Nix, J.; Finn, J., Pyrrolopyrimidine inhibitors of DNA gyrase B (GyrB) and topoisomerase IV (ParE). Part I: structure guided discovery and optimization of dual targeting agents with potent, broad-spectrum enzymatic activity. *Bioorganic & Medicinal Chemistry Letters* **2013**, *23* (5), 1529-1536; (b) Trzoss, M.; Bensen, D. C.; Li, X. M.; Chen, Z. Y.; Lam, T.; Zhang, J. H.; Creighton, C. J.; Cunningham, M. L.; Kwan, B.; Stidham, M.; Nelson, K.; Brown-Driver, V.; Castellano, A.; Shaw, K. J.; Lightstone, F. C.; Wong, S. E.; Nguyen, T. B.; Finn, J.; Tari, L. W., Pyrrolopyrimidine inhibitors of DNA gyrase B (GyrB) and topoisomerase IV (ParE), Part II: development of inhibitors with broad

spectrum, Gram-negative antibacterial activity. *Bioorg Med Chem Lett* **2013**, *23* (5), 1537-1543.

18. (a) Sherer, B. A.; Hull, K.; Green, O.; Basarab, G.; Hauck, S.; Hill, P.; Loch, J. T.; Mullen, G.; Bist, S.; Bryant, J.; Boriack-Sjodin, A.; Read, J.; DeGrace, N.; Uria-Nickelsen, M.; Illingworth, R. N.; Eakin, A. E., Pyrrolamide DNA gyrase inhibitors: optimization of antibacterial activity and efficacy. *Bioorg Med Chem Lett* **2011**, *21* (24), 7416-7420; (b) Eakin, A. E.; Green, O.; Hales, N.; Walkup, G. K.; Bist, S.; Singh, A.; Mullen, G.; Bryant, J.; Embrey, K.; Gao, N.; Breeze, A.; Timms, D.; Andrews, B.; Uria-Nickelsen, M.; Demeritt, J.; Loch, J. T.; Hull, K.; Blodgett, A.; Illingworth, R. N.; Prince, B.; Boriack-Sjodin, P. A.; Hauck, S.; MacPherson, L. J.; Ni, H. H.; Sherer, B., Pyrrolamide DNA gyrase inhibitors: fragment-based nuclear magnetic resonance screening to identify antibacterial agents. *Antimicrob Agents Ch* **2012**, *56* (3), 1240-1246; (c) Uria-Nickelsen, M.; Blodgett, A.; Kamp, H.; Eakin, A.; Sherer, B.; Green, O., Novel DNA gyrase inhibitors: microbiological characterisation of pyrrolamides. *Int J Antimicrob Ag* **2013**, *41* (1), 28-35.

19. Tomašič, T.; Katsamakas, S.; Hodnik, Ž.; Ilaš, J.; Brvar, M.; Solmajer, T.; Montalvão, S.; Tammela, P.; Banjanac, M.; Ergović, G.; Anderluh, M.; Peterlin Mašič, L.; Kikelj, D., Discovery of 4,5,6,7-tetrahydrobenzo[1,2-*d*]thiazoles as novel DNA gyrase inhibitors targeting the ATP-binding site. *J Med Chem* **2015**, DOI: 10.1021/acs.jmedchem.5b00489

20. (a) Peigneur, S.; Žula, A.; Zidar, N.; Chan-Porter, F.; Kirby, R.; Madge, D.; Ilaš, J.; Kikelj, D.; Tytgat, J., Action of clathrodin and analogues on voltage-gated sodium channels. *Mar Drugs* **2014**, *12* (4), 2132-2143; (b) Zidar, N.; Montalvao, S.; Hodnik, Ž.; Nawrot, D. A.; Žula, A.; Ilaš, J.; Kikelj, D.; Tammela, P.; Mašič, L. P., Antimicrobial activity of the marine alkaloids, clathrodin and oroidin, and their synthetic analogues. *Mar Drugs* **2014**, *12* (2), 940-963; (c) Forte, B.; Malgesini, B.; Piutti, C.; Quartieri, F.; Scolaro, A.; Papeo, G., A submarine journey: the pyrrole-imidazole alkaloids. *Mar Drugs* **2009**, *7* (4), 705-753; (d) Al Mourabit,

A.; Potier, P., Sponge's molecular diversity through the ambivalent reactivity of 2-aminoimidazole: a universal chemical pathway to the oroidin-based pyrrole-imidazole alkaloids and their palau'amine congeners. *Eur J Org Chem* **2001**, (2), 237-243.

21. Bellon, S.; Parsons, J. D.; Wei, Y. Y.; Hayakawa, K.; Swenson, L. L.; Charifson, P. S.; Lippke, J. A.; Aldape, R.; Gross, C. H., Crystal structures of *Escherichia coli* topoisomerase IV ParE subunit (24 and 43 kilodaltons): a single residue dictates differences in novobiocin potency against topoisomerase IV and DNA gyrase. *Antimicrob Agents Ch* **2004**, *48* (5), 1856-1864.

22. de Mol, N. J.; Dekker, F. J.; Broutin, I.; Fischer, M. J. E.; Liskamp, R. M. J., Surface plasmon resonance thermodynamic and kinetic analysis as a strategic tool in drug design. Distinct ways for phosphopeptides to plug into Src and Grb2 SH2 domain. *J Med Chem* **2005**, *48* (3), 753-763.

23. Kampranis, S. C.; Gormley, N. A.; Tranter, R.; Orphanides, G.; Maxwell, A., Probing the binding of coumarins and cyclothialidines to DNA gyrase. *Biochemistry-Us* **1999**, *38* (7), 1967-1976.

24. Basarab, G. S.; Manchester, J. I.; Bist, S.; Boriack-Sjodin, P. A.; Dangel, B.; Illingworth, R.; Sherer, B. A.; Sriram, S.; Uria-Nickelsen, M.; Eakin, A. E., Fragment-to-hit-to-lead discovery of a novel pyridylurea scaffold of ATP competitive dual targeting type II topoisomerase inhibiting antibacterial agents. *J Med Chem* **2013**, *56* (21), 8712-8735.

25. PyMOL, Delano Scientific LLC, San Francisco, CA, http://pymol.sourceforge.net.

26. (a) McGann, M. R.; Almond, H. R.; Nicholls, A.; Grant, J. A.; Brown, F. K., Gaussian docking functions. *Biopolymers* **2003**, *68* (1), 76-90; (b) McGaughey, G. B.; Sheridan, R. P.; Bayly, C. I.; Culberson, J. C.; Kreatsoulas, C.; Lindsley, S.; Maiorov, V.; Truchon, J. F.; Cornell, W. D., Comparison of topological, shape, and docking methods in virtual screening. *Journal of Chemical Information and Modeling* **2007**, *47* (4), 1504-1519; (c) McGann, M.,

FRED pose prediction and virtual screening accuracy. *Journal of Chemical Information and Modeling* **2011**, *51* (3), 578-596.

27. FRED version 3.0.1. OpenEye Scientific Software, Santa Fe, NM. http://www.eyesopen.com

28. Sali, A.; Blundell, T. L., Comparative protein modeling by satisfaction of spatial restraints. *Journal of Molecular Biology* **1993**, *234* (3), 779-815.

29. Notredame, C.; Higgins, D. G.; Heringa, J., T-Coffee: A novel method for fast and accurate multiple sequence alignment. *Journal of Molecular Biology* **2000**, *302* (1), 205-217.

30. Laskowski, R. A.; Macarthur, M. W.; Moss, D. S.; Thornton, J. M., Procheck - a program to check the stereochemical quality of protein structures. *J Appl Crystallogr* **1993**, *26*, 283-291.

31. (a) Sippl, M. J., Recognition of errors in 3-dimensional structures of proteins. *Proteins* **1993**, *17* (4), 355-362; (b) Wiederstein, M.; Sippl, M. J., ProSA-web: interactive web service for the recognition of errors in three-dimensional structures of proteins. *Nucleic Acids Res* **2007**, *35*, W407-W410.

32. Alt, S.; Mitchenall, L. A.; Maxwell, A.; Heide, L., Inhibition of DNA gyrase and DNA topoisomerase IV of *Staphylococcus aureus* and *Escherichia coli* by aminocoumarin antibiotics. *J Antimicrob Chemoth* **2011**, *66* (9), 2061-2069.

33. Wikler, M. A.; Cockerill, F. R.; Craig, W. A.; Dudley, M. N.; Eliopoulos, G. M.; Hecht, D. W. et al., Performance standards for antimicrobial disk susceptibility tests; approved standard - ninth edition, CLSI. 26 (2006) 1-35.

34. GAMESS interface, ChemBio3D Ultra 13.0, ChemBioOffice Ultra 13.0, CambridgeSoft.

35. Halgren, T. A., Merck molecular force field .1. Basis, form, scope, parameterization, and performance of MMFF94. *J Comput Chem* **1996**, *17* (5-6), 490-519.

36. Hawkins, P. C. D.; Skillman, A. G.; Warren, G. L.; Ellingson, B. A.; Stahl, M. T., Conformer generation with OMEGA: algorithm and validation using high quality structures from the protein databank and cambridge structural database. *Journal of Chemical Information and Modeling* **2010**, *50* (4), 572-584.

37. OMEGA version 2.4.6. OpenEye Scientific Software, Santa Fe, NM. http://www.eyesopen.com.

38. Phillips, J. C.; Braun, R.; Wang, W.; Gumbart, J.; Tajkhorshid, E.; Villa, E.; Chipot, C.; Skeel, R. D.; Kale, L.; Schulten, K., Scalable molecular dynamics with NAMD. *J Comput Chem* **2005**, *26* (16), 1781-1802.

39. MacKerell, A. D.; Bashford, D.; Bellott, M.; Dunbrack, R. L.; Evanseck, J. D.; Field, M. J.; Fischer, S.; Gao, J.; Guo, H.; Ha, S.; Joseph-McCarthy, D.; Kuchnir, L.; Kuczera, K.; Lau, F. T. K.; Mattos, C.; Michnick, S.; Ngo, T.; Nguyen, D. T.; Prodhom, B.; Reiher, W. E.; Roux, B.; Schlenkrich, M.; Smith, J. C.; Stote, R.; Straub, J.; Watanabe, M.; Wiorkiewicz-Kuczera, J.; Yin, D.; Karplus, M., All-atom empirical potential for molecular modeling and dynamics studies of proteins. *J Phys Chem B* **1998**, *102* (18), 3586-3616.

40. (a) Vanommeslaeghe, K.; Hatcher, E.; Acharya, C.; Kundu, S.; Zhong, S.; Shim, J.; Darian, E.; Guvench, O.; Lopes, P.; Vorobyov, I.; MacKerell, A. D., CHARMM General Force Field: a force field for drug-like molecules compatible with the CHARMM all-atom additive biological force fields. *J Comput Chem* **2010**, *31* (4), 671-690; (b) Vanommeslaeghe, K.; MacKerell, A. D., Automation of the CHARMM General Force Field (CGenFF) I: bond perception and atom typing. *Journal of Chemical Information and Modeling* **2012**, *52* (12), 3144-3154; (c) Vanommeslaeghe, K.; Raman, E. P.; MacKerell, A. D., Automation of the CHARMM General Force Field (CGenFF) II: assignment of bonded parameters and partial atomic charges. *Journal of Chemical Information and Modeling* **2012**, *52* (12), 3155-3168.

41. Humphrey, W.; Dalke, A.; Schulten, K., VMD: Visual molecular dynamics. *Journal of Molecular Graphics & Modelling* **1996**, *14* (1), 33-38.

42. Jorgensen, W. L.; Chandrasekhar, J.; Madura, J. D.; Impey, R. W.; Klein, M. L., Comparison of simple potential functions for simulating liquid water. *J Chem Phys* **1983**, *79* (2), 926-935.

43. Darden, T.; York, D.; Pedersen, L., Particle mesh Ewald: an *N*-log(*N*) method for Ewald sums in large systems. *J Chem Phys* **1993**, *98* (12), 10089-10092.

44. Ryckaert, J. P.; Ciccotti, G.; Berendsen, H. J. C., Numerical integration of cartesian equations of motion of a system with constraints: molecular dynamics of *n*-alkanes. *J Comput Phys* **1977**, *23* (3), 327-341.

45. Caesar, J. C.; Griffiths, D. V.; Griffiths, P. A.; Tebby, J. C., Reactions of ylides formed from trialkyl phosphites with dialkyl acetylenedicarboxylates in the presence of carbon dioxide. *J Chem Soc Perk T 1* **1990**, (8), 2329-2334.

46. Miyatake, K.; Kaga, S., Studies on hippuric acid derivatives. II. Synthesis of aminohippuric acids. *Yakugaku Zasshi* **1952**, *72* (9), 1160-1161.

47. Oguchi, M.; Wada, K.; Honma, H.; Tanaka, A.; Kaneko, T.; Sakakibara, S.; Ohsumi, J.; Serizawa, N.; Fujiwara, T.; Horikoshi, H.; Fujita, T., Molecular design, synthesis, and hypoglycemic activity of a series of thiazolidine-2,4-diones. *J Med Chem* **2000**, *43* (16), 3052-3066.

48. Kaye, I. A.; Burlant, W. J.; Price, L., Thiocyanation of *p*-dialkylaminoalkoxyanilines. *J Org Chem* **1951**, *16* (9), 1421-1426.

49. Martin, M. W.; Newcomb, J.; Nunes, J. J.; McGowan, D. C.; Armistead, D. M.; Boucher, C.; Buchanan, J. L.; Buckner, W.; Chai, L.; Elbaum, D.; Epstein, L. F.; Faust, T.; Flynn, S.; Gallant, P.; Gore, A.; Gu, Y.; Hsieh, F.; Huang, X.; Lee, J. H.; Metz, D.; Middleton, S.; Mohn, D.; Morgenstern, K.; Morrison, M. J.; Novak, P. M.; Oliveira-Dos-

Santos, A.; Powers, D.; Rose, P.; Schneider, S.; Sell, S.; Tudor, Y.; Turci, S. M.; Welcher, A. A.; White, R. D.; Zack, D.; Zhao, H. L.; Zhu, L.; Zhu, X. T.; Ghiron, C.; Amouzegh, P.; Ermann, M.; Jenkins, J.; Johnston, D.; Napier, S.; Power, E., Novel 2-aminopyrimidine carbamates as potent and orally active inhibitors of Lck: synthesis, SAR, and in vivo antiinflammatory activity. *J Med Chem* **2006**, *49* (16), 4981-4991.

50. Moraski, G. C.; Chang, M.; Villegas-Estrada, A.; Franzblau, S. G.; Mollmann, U.; Miller, M. J., Structure-activity relationship of new anti-tuberculosis agents derived from oxazoline and oxazole benzyl esters. *Eur J Med Chem* **2010**, *45* (5), 1703-1716.

51. Baell, J. B.; Holloway, G. A., New substructure filters for removal of pan assay interference compounds (PAINS) from screening libraries and for their exclusion in bioassays. *J Med Chem* **2010**, *53* (7), 2719-2740.

## Table of contents graphic